MINISTRY OF EDUCATION & RESEARCH

National University of Science & Technology POLITEHNICA Bucharest

PhD School Biotechnical Engineering Systems

Eng. Florin-Marian NEAGOE

ABSTRACT Ph.D. THESIS

Scientific Coordinator:

Prof. Habil. PhD Eng. Mihai BUGARU (NUSTPB)

2023

National University of Science & Technology POLITEHNICA Bucharest

PhD School Biotechnical Engineering Systems

ABSTRACT-Ph.D. Thesis

Contributions to Theoretical & Experimental Investigations of Noise Barriers

Scientific Coordinator:

Prof. Habil. PhD Eng. Mihai BUGARU

Ph.D. Student:
Eng. Florin-Marian NEAGOE

BUCHAREST

2023

Content

Chapter 1. State of the Art concerning theoretical & experimental research in the field of automotive noise attenuation using acoustic barriers.

After detailing the EU-Regulations in the field of automotive noise attenuation using acoustic barriers, Chapter One deals with the state of the art in this specific field.

The Ph.D. thesis is structured into six chapters:

- Chapter 1. State of the Art concerning theoretical & experimental research in the field of automotive noise attenuation using acoustic barriers,
- Chapter 2. Anechoic lab investigations concerning noise attenuation using acoustic barriers,
- Chapter 3. In situ investigations concerning noise attenuation using acoustic barriers,
- Chapter 4 . Modeling noise attenuation using acoustic barriers,
- Chapter 5. Optimization of asymmetric edge diffraction on the top of acoustic barriers for industrial and automotive/railway traffic noise attenuation,
- Chapter 6. Final conclusions. Contributions. Directions for future research.

In Chapter 2, the acoustic properties of several materials were determined using experiments carried out in the Anechoic Chamber. To realize this goal, an experimental panel having the geometry 2m x 1.5 m x 1m, was used.

Chapter 3 reveals the results obtained in situ for different types of materials inserted in the considered panel.

Chapter 4 presents a detailed modeling analysis for noise attenuation by employing four different approaches: Maekawa-Tatge Method[G.R.9 –10], Kurze&Anderson formulation [G.R..11], General Prediction Method(GPM) [R.C.4.1, R.C.4.2] and Menounou Formulation [G.R.12]. The analysis reveals that the best approach is the Modified General Prediction Method(MGPM).

Chapter 5 investigates the optimization of asymmetric edge diffraction mounted on the top of the acoustic design for industrial noise attenuation as well as for automotive/railway traffic noise attenuation. The method of prediction was considered a modified version of MGPM.

Chapter 6 presents the final conclusions, the contributions, and the future research directions.

The method of noise attenuation prediction is GPM, based on ISO 9613. This method was modified considering the next aspects:

- down-wind meteorological effect,

- noise atmospheric attenuation, generated by relaxation frequencies of oxygen and nitrogen in the air, temperature, air humidity, atmospheric pressure,

- noise ground absorptions-reflections effects,

- edge noise diffraction effects.

Chapter 2. Anechoic lab investigations concerning noise attenuation using acoustic barriers

The Chapter is based on the published articles [GR.20, GR21]. The paper reveals the experimental research carried out, in the anechoic chamber at the Department of Mechanics of University POLITEHNICA of Bucharest, to highlight the noise reduction (the acoustic attenuation) from the source (S) to the receiver (R), using different material layers for the noise barrier. The tests were performed on an experimental model having the dimensions 2mx1.5m, considering an incident wave angle of the source with respect to the receiver, having initially a diffraction angle of 0^0 (in the shadow field, orthogonal on the plane of the barrier), subsequently with a diffraction angle of $\pm 45^0$ (angle of the receiver with respect to the direct straight angle of the source). The experimental results are presented as a function of the internal layers of the barrier's structure as well as a function of the incident diffraction angle of the sound wave. The conclusion of the paper reveals the basic differences obtained by this experimental research.

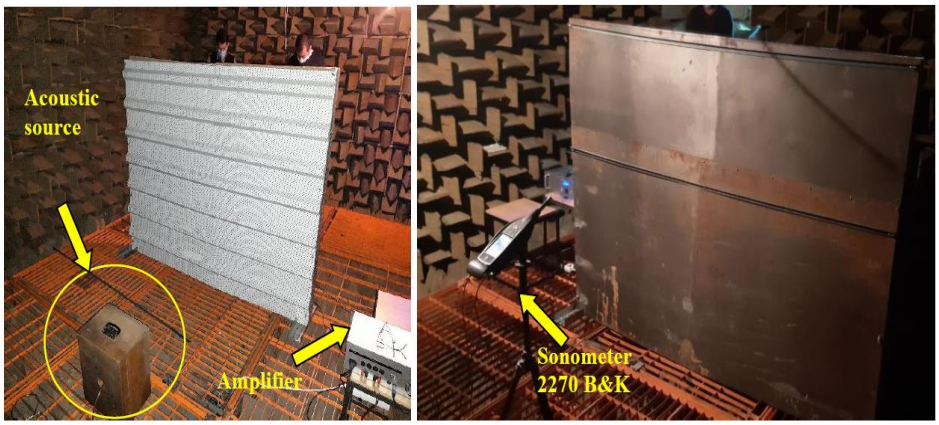

Fig..2.1. Photos during the tests. [G.R.20; G.R.21]

The noise barrier is made as a sandwich panel with a profiled steel sheet at the exterior having a width of 0.8 mm, with perforations towards the noise source and the global 2000 mm x 1500 mm, while the steel sheet towards the receiver is plane and without perforations. This structure is fixed into a frame composed of two steel U-profile columns with perforations, as can be seen in Figure 2.3. Inside, this sandwich structure contains one central OSB plate having the dimensions 2000 mm x 1500 mm x 15 mm as core and two sheets of phono-absorbent material, one on every side of the OSB core, having the dimensions 2000 mm x 1500 mm x 40 mm, as can be seen in Figure 2.3. To establish the noise attenuation efficiency as a function of the structure of the noise barrier, three kinds of different materials having the same width of 40 mm as in Figure 2.4:

case 1 – expanded polyethylene,

case 2 – recycled polyurethane foam, having a density of 90 Kg/m^3 (with60% flakes of flexible polyurethane foam, 30% textile materials, and 10 % binder glue),

case 3 – basaltic wool.

For acoustical data, it was used as an acoustic source (S) a loudspeaker connected to an amplifier, and a generator of white noise. The noise level was measured in the nearby vicinity of the source in the opposite side of the barrier, at different points of receiving (R_i), using a sonometer Model 2270 Brüel & Kjær. All the data were transferred to a computer to be processed.

Fig. 2.3. Structure detail of the noise barrier model[G.R.20; G.R.21]

a. b. c.

Fig. 2.4. Types of materials used for phono absorption[G.R.20; G.R.21]:
a. case 1-expanded polyethylene, b. case 2-recycled polyurethane foam, c. case 3 – basaltic wool.

The sonometer used for data recording was placed near the noise source (S) and then in different positions of the receiver (Ri) at distances of 0.5 m, 1 m, and 2 m with respect to the barrier at a variable height of 0.5 m; 1 m; 1.5 m from the ground, on the orthogonal direction to the barrier and inclined with ± 45^0 to this direction, being done 21 recordings for each case 1 to 3. All the elements were placed on a steel lattice at 0.5 m height above the phono-absorbing surface of the anechoic chamber.

The scheme of all measuring positions is presented in Figure 2.5.

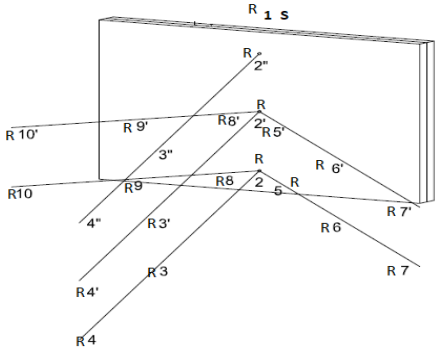

Fig. 2,5. Scheme of measuring positions. [G.R.20; G.R.21]

For a better understanding all the notations as well as the geometric disposal of measuring points

in Figures 2.6-2.8 present the details, for the incident directions with respect to the source position at 0^0 and respectively at $\pm 45^0$. The positions of measuring points presented in Figure 2.6, at an incident angle of 0^0, are:

- R1 is placed at a 0,5 m with respect to the noise source (S) at a height of 0,5 m above the lattice,
- R2, R2', R2" are the measuring positions placed at a distance of 0,5 m with respect to the barrier and at a variable height of 0,5 m, 1 m, and 1,5 m above the lattice,
- R3, R3', R3" are the measuring positions at 1 m with respect to the noise barrier and at variable heights of 0,5 m, 1 m, and 1,5 m above the lattice,
- R4, R4', and R4" are the measuring positions at 2 m with respect to the noise barrier and at variable heights of 0.5 m, 1 m, and 1.5 m above the lattice.

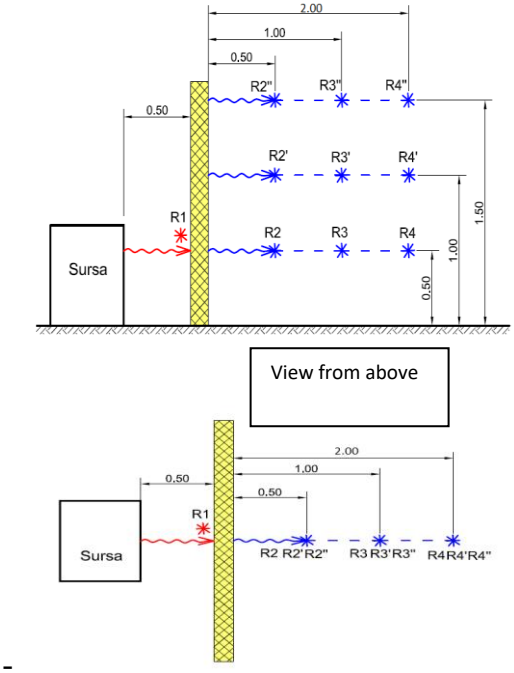

Fig. 2.6. Positions of the measuring points for an incident angle of 0^0 (lateral view; view from above).

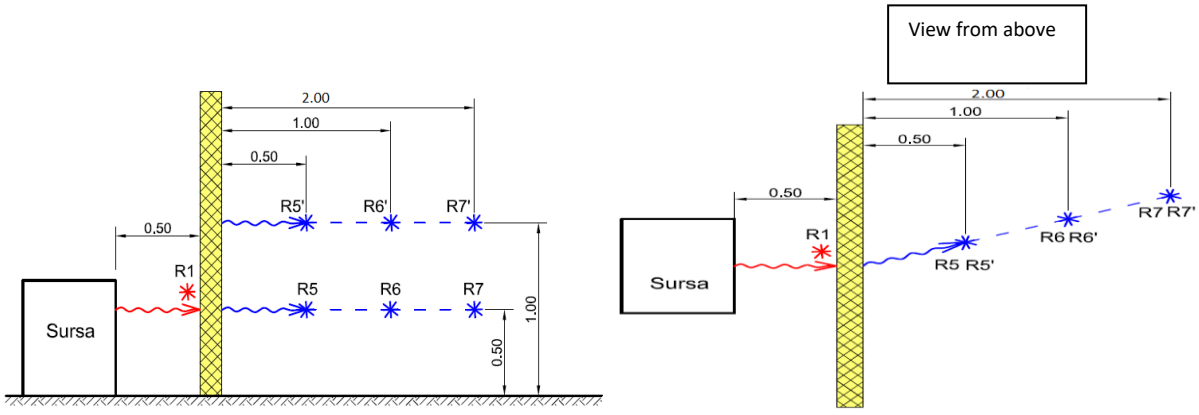

Fig. 2.7. Positions of the measuring points for an incident angle of $+45^0$ (lateral view; view from above).

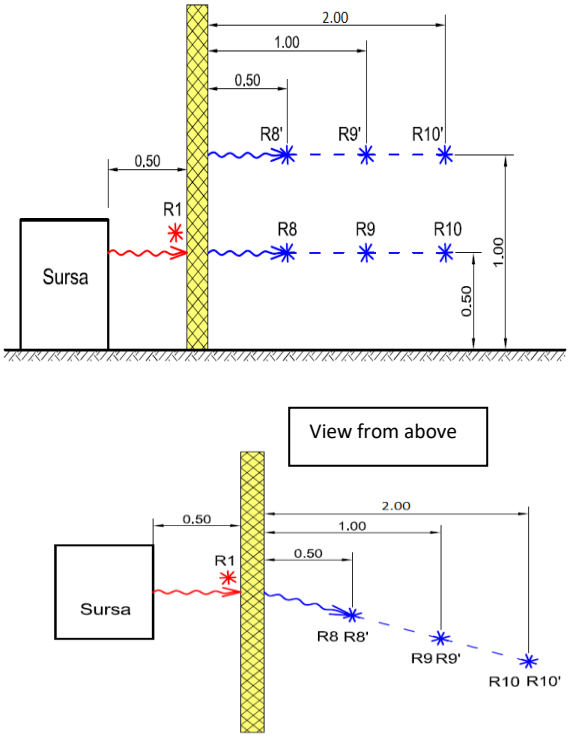

Fig. 2.8. Positions of the measuring points for an incident angle of -45^0 (lateral view; view from above).

The positions of measuring points presented in Figure 2.7, at an incident angle of +45^0, are:

- R1 is placed at a 0,5 m with respect to the noise source (S) at a height of 0,5 m above the lattice,
- R5, R5' are the measuring positions placed at 0,5 m with respect to the barrier and at a variable height of 0,5 m and 1 m above the lattice,
- R6, R6' are the measuring positions placed at 1 m with respect to the barrier and at a variable height of 0,5 m and 1 m above the lattice,
- R7, R7' are the measuring positions placed at 2 m with respect to the barrier and at a variable height of 0.5 m and 1 m above the lattice.

The positions of measuring points presented in Figure 2.8, at an incident angle of -45^0, are:

- R1 is placed at a 0,5 m with respect to the noise source (S) at a height of 0,5 m above the lattice,
- R8, R8' are the measuring positions placed at 0,5 m with respect to the barrier and at a variable height of 0,5 m and 1 m above the lattice,
- R9, R9' are the measuring positions placed at 1 m with respect to the barrier and at a variable height of 0,5 m and 1 m above the lattice,
- R10, R10' are the measuring positions placed at 2 m with respect to the barrier and at a variable height of 0.5 m and 1 m above the lattice.

Experimental data for case 1

In case 1 for which it was used as acoustic phono absorbent material the expanded polyethylene, see Figure 2.4.a., with an angle of incidence of 0^0 with respect to the orthogonal direction on the surface of the noise barrier, see Figure 5, the experimental data are presented in Figure 2.9. To highlight the position of the noise source (S), denoted R1, it is considered in a horizontal direction, at -0.5 m (in front of the barrier) on the left-hand side. The other measuring positions R2, R2' …

R4", are in the backside of the, at distances mentioned above on the right-hand side of the barrier (positive values for the distances). The experimental data, to highlight the variation of acoustic level for case 1, at an inclined incidence angle of $\pm 45^0$, see figures 2.7- 2.8, are presented in Figure 2.10.

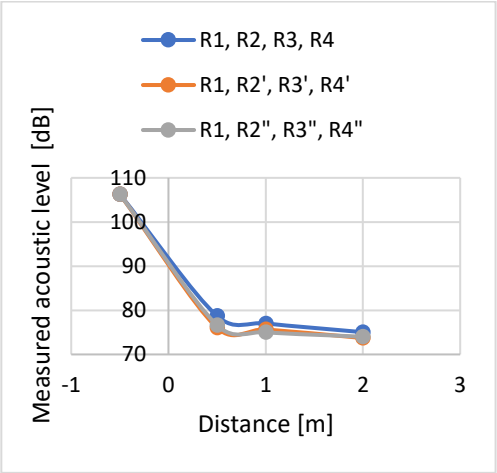

Fig. 2.9.Variation of acoustic level, case 1, angle of incidence of 0^0.

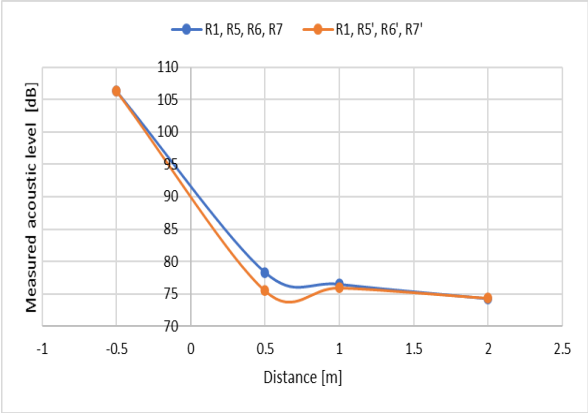

a. angle of incidence $+45^0$

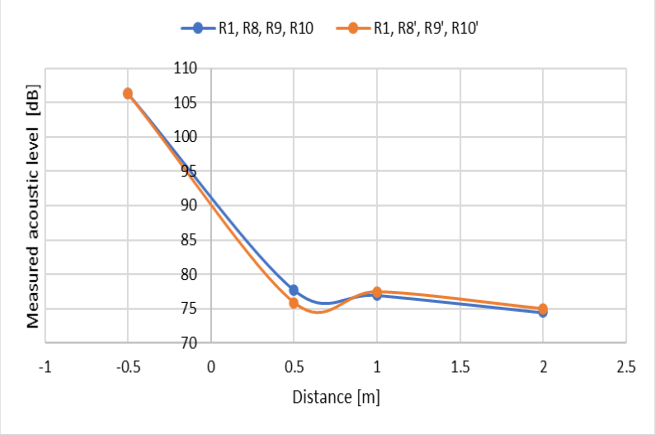

b. angle of incidence -45^0

Fig. 2.10. Variation of acoustic level for the case 1, at incidence angles $\pm 45^0$

Due to the geometric form of the acoustic barrier, with respect to the position of the noise source (S), in Figure 2.10 the variations of the acoustic level at incident angles of $\pm 45^0$ are similar.

Experimental data for case 2

In case 2, when the structure of the noise barrier uses acoustic phono absorbent material recycled polyurethane foam(case 2), see Figure 2.4.b for the incident angle of 0^0, as in Figure 2.6, the experimental data are presented in Figure 2.11.

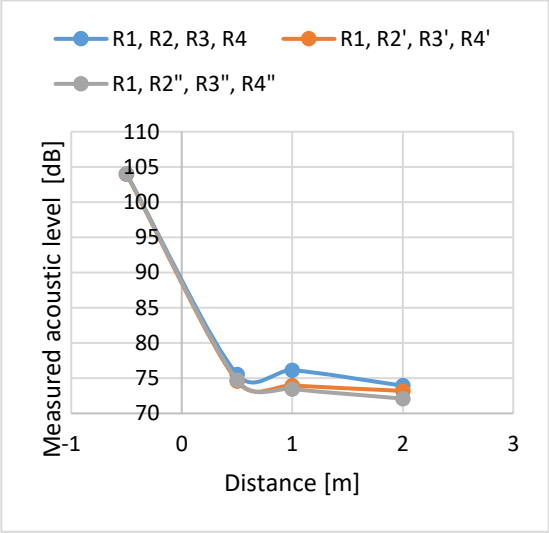

Fig. 2.11. Variation of acoustic level, case 2, angle of incidence of 0^0.

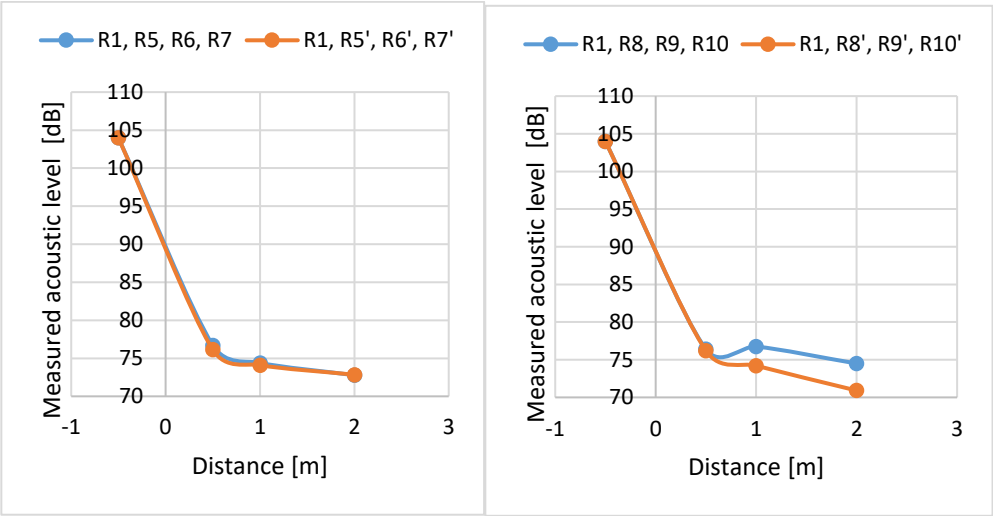

a. angle of incidence $+45^0$ b. angle of incidence -45^0

Fig. 2.12. Variation of acoustic level for the case 2, at incidence angles $\pm 45^0$

The experimental data, to highlight the variation of acoustic level for case 2, at an inclined incidence angle of $\pm 45^0$, see figures 2.7-2.8, are presented in Figure 2.12. Due to the geometric form of the acoustic barrier, with respect to the position of the noise source (S), in Figure 2.12 the variations of acoustic level at incident angles of $\pm 45^0$ are similar.

Experimental data for case 3

In case 3, when the structure of the noise barrier uses an acoustic phono-absorbent material recycled polyurethane foam(case 3), see Figure 2.4.c for the incident angle of 0^0, as in Figure 2.6, the experimental data are presented in Figure 2.13. The experimental data, to highlight the variation of acoustic level for case 3, at an inclined incidence angle of $\pm 45^0$, see Figures 2.7-2.8, are presented in Figure 2.14.

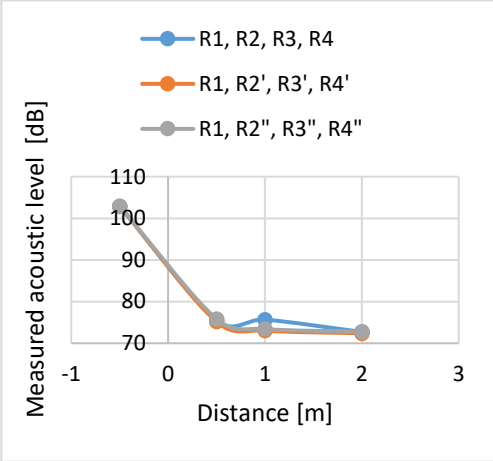

Fig. 2.13. Variation of acoustic level, case 3, angle of incidence of 0^0.

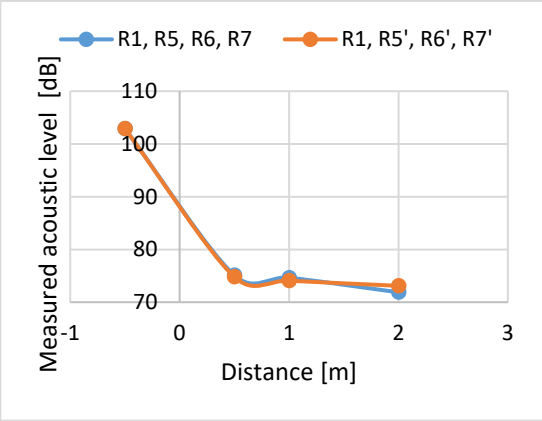

a) angle of incidence $+45^0$

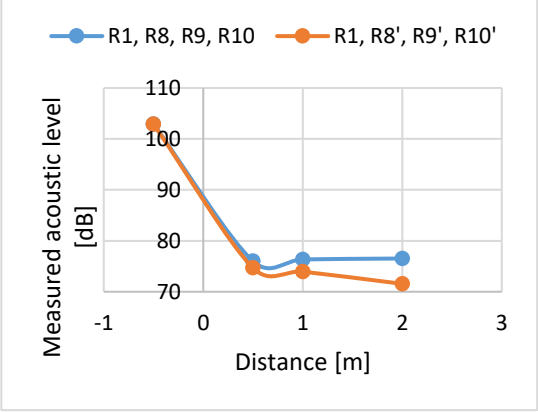

b) angle of incidence -45^0

Fig. 2.14. Variation of acoustic level for the case 3, at incidence angles $\pm 45^0$

Due to the geometric form of the acoustic barrier, with respect to the position of the noise source (S), in Figure 2.14 the variations of the acoustic level at incident angles of $\pm 45^0$ are similar.

The experimental data were not altered by the adjacent noise and by using the anechoic chamber were avoided the multiple reflections. The recordings, done on a short period of time, in the range of one-third of an octave, pondered on the reference level A, were presented only as global equivalent acoustic levels L_{Aeq}, as a variation between the level of measured acoustic data at source (S, R1) and the level of measured acoustic data at different receiving points (R2, R3, …, R10'). To define the acoustic parameters, it was considered the next terms [R.C.2.7; R.C.2.8]:

$$L_{Aeq} = 10\log\left[\frac{1}{T_0}\int_{t_1}^{t_2}\frac{p_A^2(t)}{p_0^2}dt\right] \quad (2.1)$$

where: $p_A(t)$ is the pondered instantaneously acoustic pressure, p_0 is the reference pressure, having the value 20, $(t_2 - t_1)$ is the period of time measuring, the selected value is 15 s, T_0 is the reference time, having the value of 1 s. In correlation with the indirect measuring method[R.C.2.7], when the data of acoustic pressure are collected before and after the presence of a noise barrier because the distances are relatively short, it can be approximated the noise attenuation of the barrier or the loss of insertion as:

$$\Delta L_i = L_S - L_{Ri}\ [dB(A)] \quad (2.2)$$

where L_S is the sound pressure level near the acoustic source (S, R1) and L_{Ri} is the sound pressure level measured in the receiving positions R2, R3, …, R10'. In tables 1 to 3 is presented the computation of acoustic attenuation for the cases considered being split for variable heights at 0.5 m, 1 m, and 1.5 m above the lattice.

Table 1. Acoustic attenuation at the height of 0,5 m Table 2. Acoustic attenuation at the height of 1 m

ΔL_i	ΔL_2	ΔL_3	ΔL_4	ΔL_5	ΔL_6	ΔL_7	ΔL_i	$\Delta L_{5'}$	$\Delta L_{6'}$	$\Delta L_{7'}$	$\Delta L_{8'}$	$\Delta L_{9'}$	$\Delta L_{10'}$
Case1	27.58	29.27	31.26	28	29.8	**32.04**	Case1	30.82	30.33	31.92	30.45	28.84	31.32
Case 2	28.44	27.88	30.06	27.28	29.59	**31.22**	Case 2	27.86	29.89	31.16	27.79	29.79	**33.09**
Case 3	27.4	27.22	30.16	27.78	28.26	**31.02**	Case 3	28.09	28.82	29.79	28.22	28.96	**31.35**

Table 3. Acoustic attenuation at the height of 1,5 m

ΔL_i **[dB(A)]**	ΔL_2	ΔL_3	ΔL_4
Case1	29.67	31.27	**32.29**
Case 2	29.25	30.53	**31.9**
Case 3	27.07	29.46	**30.14**

The maximum values in these tables are bolded to highlight them. In Table 1, it can be remarked that in all the cases for the height of 0.5 m, the maximum values of attenuation correspond to the point R7, that is at a 2 m distance from the barrier at an inclined incidence angle of $+45^0$. Also, in Table 2, it can be remarked that the maximum values are for a height of 1 m, above the lattice for case 1 at $\Delta L_{4'}$, which corresponds to the point R4' and at $\Delta L_{10'}$, for cases 2 to 3, see point R10', in figure 7, at an inclined incidence angle of -45^0. In conclusion, based on the obtained data, can be remarked a strong efficiency of the acoustic barrier at an inclined incidence angle of $\pm 45^0$, this being justified not by numerical modeling.

Chapter 3. In situ investigations concerning noise attenuation using acoustic barriers

The noise generated by automotive traffic is produced by the following phenomena:

- noise generated by the collisions between wheels and road surface,
- automotive aerodynamic noise,
- noise induced by automotive engines,
- random impact noise induced by mechanical systems transmission.

The present chapter deals with in situ experiments regarding noise attenuation using acoustic sandwich barriers made with different acoustic insulating materials. The measurements were performed using B&K 2270 to measure the acoustic noise level.

An important rule is to place the acoustic barrier as close to the source so that the geometric condition is satisfied, $r_s \leq H$, r_s being the distance to the source(for the acoustic barrier), and H being the height of the barrier.

At a distance of 2.5m from the exterior of the highway the noise level was 82.71 dB. Wind speed was approximately 18 km/h, and temperature was 10-12^{0}C.

Fig..3.1 Photographs during tests

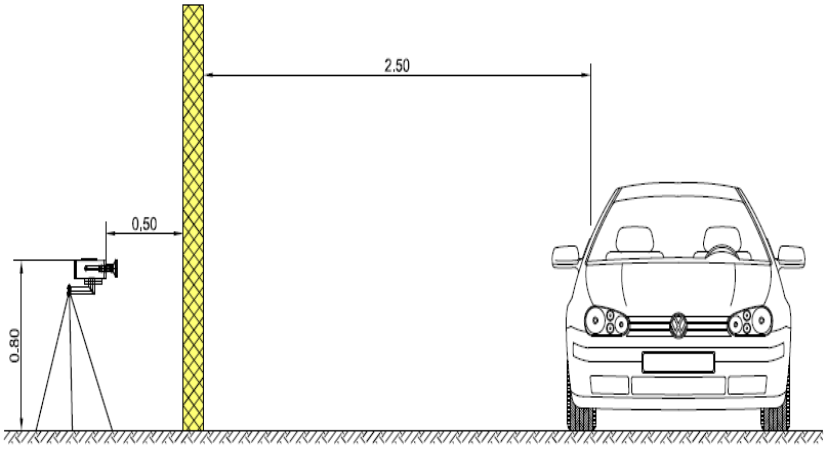

Fig..3.2 Measuring scheme

Panel: Bazaltic wool– OSB – Bazaltic wool

Tabel.3.1. Experimental data

No.	LAeq [dB]		Panel type
	Measurement height–0.8m	Measurement height -0.5m	
1	R_1-77.92 dB		Bazaltic wool– OSB – Bazaltic wool

Panel: Bazaltic wool– OSB – Polyurethane foam

Tabel.3.2. Experimental data

No.	Source distance 2.5 m (in front panel)		Distance behind barrier
	Measurement height–0.8m	Measurement height -0.5m	Panel type
2	R_2-77.82 dB		Bazaltic wool– OSB – Polyurethane foam

Panel: Polyurethane foam -OSB- Polyurethane foam

Tabel.3.3. Experimental data

No.	LAeq [dB]		Panel type
	Measurement height–0.8m	Measurement height -0.5m	
3	R_3-79.72 dB		Polyurethane foam -OSB- Polyurethane foam

Panel: Polyurethane foam – OSB – expanded polyethylene

Tabel.3.4. . Experimental data

No.	LAeq [dB]		Panel type
	Measurement height–0.8m	Measurement height -0.5m	
4	R_4-77.61 dB		Polyurethane foam – OSB – expanded polyethylene

Panel: E**xpanded polyethylene** – **OSB** – E**xpanded polyethylene**

Tabel.3.5. . Experimental data

No.	**LAeq [dB]**		**Panel type**
	Measurement height–0.8m	**Measurement height -0.5m**	
5	R_5-78.22 dB		**E**xpanded polyethylene **– OSB –** **E**xpanded polyethylene

As can be seen from the Tabels 3.1-3.5 noise attenuation, as a material function is in the range [3…5] dB.

The noise attenuation for each materials is given bellow:

- **Noise attenuation using the panel with the structure: Bazaltic wool– OSB – Bazaltic wool**

$$\Delta L=82.71 \text{ dB} - 77.92 \text{ dB} = 4.79 \text{ dB}$$

- **Noise attenuation using the panel with the structure: Bazaltic wool– OSB – Polyurethane foam**

$$\Delta L=82.71 \text{ dB} - 77.82 \text{ dB} = 4.89 \text{ dB}$$

- **Noise attenuation using the panel with the structure: Polyurethane foam -OSB- Polyurethane foam**

$$\Delta L=82.71 \text{ dB} - 79.72 \text{ dB} = 2.99 \text{ dB}$$

- **Noise attenuation using the panel with the structure: Polyurethane foam – OSB – expanded polyethylene**

$$\Delta L=82.71 \text{ dB} - 77.61 \text{ dB} = 5.1 \text{ dB}$$

- **Noise attenuation using the panel with the structure:** E**xpanded polyethylene** – **OSB** – E**xpanded polyethylene**

$$\Delta L=82.71 \text{ dB} - 78.22 \text{ dB} = 4.49 \text{ dB}$$

During the investigations it was evaluated the acoustic performance of such panels regarding the following aspects:

- distance between the source and the acoustic barrier,
- distance between the acoustic barrier and the receptor.

Based on the ISO Standards (En1438; EN14389-1, EN 1793-1 ; EN 1793-2) [R.C.3.1; R.C.3.2; R.C.3.3; R.C.3.4] the acoustic performance of insulated materials has the following basis:

- acoustic element,
- insulating element,
- stability and liability.

Also, the acoustic barriers must resist specific meteorological conditions such as moisture, rain, snow, ice, low temperature (under -20^0C) and high temperature (over 40^0C).

Chapter 4 . Modeling noise attenuation using acoustic barriers

The aim of the research is to provide a better prediction for noise attenuation using thin rigid barriers. Therefore, the paper presents an analysis of four methods of computing the noise attenuation for acoustic barriers: Maekawa-Tatge formulation[G.R.9 – G.R.10], Kurze&Anderson algorithm[G.R.11], Menounou formulation[G.R.12] and General Prediction Method (GPM-ISO 9613) [R.C.4.1; R.C.4.2]. In this way it was optimized the prediction computation of the noise attenuation for an acoustic barrier improved the GPM by considering new effects such as attenuation due to geometrical divergence, ground absorption-reflections, and atmospheric absorption. The new method MGPM (Modified GPM) was tested for the optimization of a y-shape edge geometry of the noise barrier, and it was found a close agreement with the experimental data published in the literature. The specific y-shape edge geometry of the noise barrier contributes to the attenuation due to diffraction phenomena. This aspect is based on the Kirchhoff diffraction theory that contains the Huygens-Fresnel theory applied to a semi-infinite acoustic barrier. The new method MGPM of predicting the noise attenuation for acoustic barriers is considering the next phenomena: the effect of the relative position of the receiver, the effect of the proximity of the source or receiver to the midplane of the barrier, the effect of the proximity of the receiver to the shadow boundary, the effects of ground absorption-reflections, the effects of atmospheric absorption and the meteorological effects due to downwind. The conclusion of the chapter reveals the optimization of the method for computing the noise attenuation using acoustic barriers, involving the corrections needed to be done for ISO-9613 and the SoundPLAN software as well as the optimization on a case study of a specific geometry of the edge barrier.

Figure 4.1 presents a semi-infinite thin barrier having: the height H, on the left side an acoustic source S at the distance ds from the barrier, on the right side a receiver R at the height y_R and at the distance x_R. We consider that the source produces only pure tones and is at 0.5 m over the ground. If we choose the plane referential system with the x-axis being at the "ground zero" horizontal and the y-axis passing through S and being vertical, then the coordinates of the receiver are R ($x_R + ds$, y_R) with respect to the system coordinates. Based on the Kirchhoff-Fresnel diffraction theory [G.R.8] the Fresnel numbers of the source S and the image of the source S' (the symmetric geometric point with respect to the plane of the barrier) are N_1 and N_2 given by the relations:

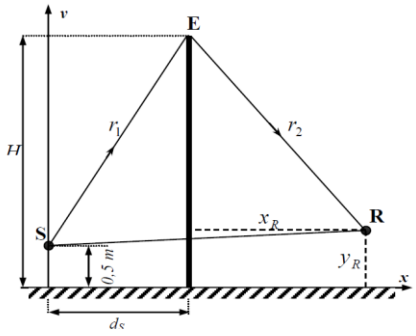

Fig.4.1 Diffraction of sound by a thin barrier. [G.R. 22; G.R.9]

$$N_1 = \frac{2\delta_1 f}{c} = \frac{k}{\pi}\left(r_1 + r_2 - d_1\right) \tag{4.1}$$

$$N_2 = \frac{2\delta_2 f}{c} = \frac{k}{\pi}\left(r_1 + r_2 - d_2\right) \tag{4.2}$$

where f is the frequency in Hz of a pure tone, c is the sound velocity in the air, and δ_1 and δ_2 are the differences between the diffraction path S-E-R and the shortest path S-R respectively S'-R given by the relations:

$$\delta_1 = r_1 + r_2 - \sqrt{\left(d_s + x_R\right)^2 + \left(y_R - 0{,}5\right)^2} = r_1 + r_2 - d_1 \tag{4.3}$$

$$\delta_2 = r_1 + r_2 - \sqrt{\left(x_R - d_s\right)^2 + \left(y_R - 0{,}5\right)^2} = r_1 + r_2 - d_2 \tag{4.4}$$

The attenuation of a thin rigid barrier given by Maekawa-Tatge formulation [G.R.9], based only on the source Fresnel number N_1, is:

$$A_b^{Ma} = 10\log_{10}\left(3 + 20N_1\right) \tag{4.5}$$

A better approach was given by Kurze and Anderson [R.C.4.3], based on the same source Fresnel number N_1, the relation of the sound pure tones attenuation with a thin rigid barrier is:

$$A_b^{KA} = 20\log_{10}\left(\frac{\sqrt{2\pi N_1}}{\tanh\sqrt{2\pi N_1}}\right) + 5 \tag{4.6}$$

The GPM provides a relation for the sound attenuation based on a modified Fresnel number N_1 as mentioned in ISO 9613-2 [G.R.17], taking into consideration a correction factor for downwind meteorological effects Kmet, given by the:

$$K_{met} = e^{-\frac{1}{2000}\sqrt{\frac{r_1 r_2 d_2}{2\delta_1}}} \tag{4.7}$$

With this correction factor K_{met} the modified Fresnel number N_1' of the source is:

$$N_1' = 0.5 N_1 K_{met} \tag{4.8}$$

and therefore, the sound attenuation of a thin rigid barrier, considered by GPM is:

$$A_b^{GPM} = 10\log_{10}\left(3 + 20N_1'\right) \tag{4.9}$$

The GPM is used in the software SoundPLAN for predicting the sound attenuation for rigid thin barriers. As can be seen, the relation (4.9), given by GPM, is like the Maekawa-Tatge approach for sound attenuation, given by relation (4.5).

The Menounou formulation [G.R.12] for the sound attenuation of a thin rigid barrier is the most complex approach because it takes into consideration both Fresnel numbers by involving the next effects: the relative position of the receiver from the source (involving only the Fresnel number N_1), the proximity of the source or the receiver to the midplane (involving the ratio N_2 /N_1), the proximity of the receiver to the shadow boundary (involving both Fresnel numbers N_1 and N_2), the diffraction effect due to spherical incident waves. The noise attenuation for a semi-infinite rigid barrier, using the Menounou formulation, considering pure tones, is given by the relation:

$$A_b^{Me} = A_b^1 + A_b^2 + A_b^3 + A_b^4 \tag{4.10}$$

where the sound attenuation given by the effect of the relative position of the receiver from the source is:

$$A_b^1 = 20\log_{10}\left(\frac{\sqrt{2\pi N_1}}{\tanh\sqrt{2\pi N_1}}\right) - 1 \tag{4.11}$$

the sound attenuation given by the effect of the proximity of the source or the receiver to the midplane is:

$$A_b^2 = 20\log_{10}\left[1 + \tanh\left(0.6\log_{10}\frac{N_2}{N_1}\right)\right] \tag{4.12}$$

the sound attenuation given by the effect of the proximity of the receiver to the shadow boundary is:

$$A_b^3 = \left[6\tanh\sqrt{N_2} - 2 - A_b^2\right]\left[1 - \tanh\sqrt{10N_1}\right] \tag{4.13}$$

and the sound attenuation given by the diffraction effect due to spherical incident waves is:

$$A_b^4 = 10\log_{10}\left[\left(\frac{r_1 + r_2}{d_1}\right)^2 + \frac{r_1 + r_2}{d_1}\right] \tag{4.14}$$

The most used method of predicting noise attenuation is GPM [R.C.4.2.] because ISO 9613-2 prescribes the model of attenuation. However, this method must be improved considering at least two phenomena: the ground absorption-reflections and the atmospheric absorption. To consider the attenuation introduced by ground absorption-reflections it was used the most convenient model, Delany-Bazley [R.C.4.13]. This model takes into consideration the effective flow resistivity of the ground σ_e and the frequency of the pure tone sound f, modifying the propagation constant k (known as wave number) of the sound in the air, given by the frequency of the pure tones and the sound speed in the air c, that normal is:

$$k = \frac{\omega}{c} = \frac{2\pi f}{c}, \tag{4.15}$$

by an empirical factor α_{gr}, so that the modified propagation constant is given by the relation

:

$$k = \frac{k}{|\alpha_{gr}|} \tag{4.16}$$

where α_{gr} is

$$\alpha_{gr} = 1 + 0.0978\left(\frac{f}{\sigma_e}\right)^{-0.700} - i0.189\left(\frac{f}{\sigma_e}\right)^{-0.595}, i = \sqrt{-1}\ . \tag{4.17}$$

By this way, the Fresnel numbers N_1 and N_2, given by the relations (4.1) and (4.2), are modified accordingly to relations (4.15) - (4.17).

The atmospheric absorption is considered using the Larsson model [G.R.14] that considers the next effects: sound frequency, air humidity, air temperature, and pressure using an attenuation coefficient α_{aa}, expressed in dBA/m, given by the relation:

$$\alpha_{aa} = f^2\left[\left(\frac{T_O}{T}\right)^{2.5}\left(\frac{0.10680e^{-3352/T} f_{r,N}}{f^2 + f_{r,N}^2} + \frac{0.01278e^{-2239.1/T} fr,O}{f^2 + f_{r,O}^2}\right) + \left(\frac{1.84x10^{-11}}{\left(\frac{T_O}{T}\right)^{0.5}\frac{p_S}{p_O}}\right)\right] \tag{4.18}$$

where f is the sound frequency, T is the absolute temperature of the atmosphere in Kelvin^0, T_0 = 293.15 K, p_s is the atmospheric pressure, p_0 =101.325 kPa, $f_{r,N}$ and $f_{r,O}$ are relaxation frequencies associated with the vibration of nitrogen and oxygen molecules. The sound attenuation due to atmospheric absorption, in the case of a rigid thin barrier (see Figure 4.1), is

$$A_\alpha = \alpha_{aa}\left(r_1 + r_2\right) \tag{4.19}$$

Taking into consideration this effect as well as the ground absorption, after correcting the Fresnel numbers N_1 and N_2 that were used in the relations (4.5), (4.6), (4.8) - (4.14) by using relations (4.16) and (4.17), it is necessary to add the correction given by the relations (18) and (19) in the modified relations (5), (6), (9) and (10). Based on ISO 9613-1[R.C.4.9] Figure 4.2 presents the sound attenuation at 30 meters distance between the source and receiver as a function of sound frequency and the relative humidity of the air at several frequencies of the pure tones (2 kHz-10 kHz).

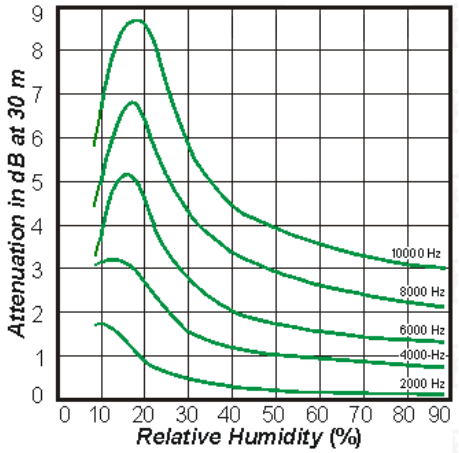

Fig. 4.2. Sound attenuation as a function of sound frequency and relative humidity

As can be seen from Fgures 4.3 and 4.4 Maekawa-Tatge approach and Kurze-Anderson algorithm are approximately the same while the GPM approach gives a difference with less 3-3.5 dBA with respect to the first 2 methods, while the Menounou method gives an "over attenuation". In the Figures 4.3 and 4.4 are presented the sound attenuation [dBA] of pure tones for an acoustic rigid semi-infinite thin barrier having a height over the ground of 3 meters, the source S is placed at the distance of 3.5 meters from the barrier at a height of 0.5 meters over the ground, the receiver R is placed at a varying distance from the barrier 0.15 to 35 meters at a height of 1.0 meters over the ground for different frequencies of the sound 100 Hz, 250 Hz, 500 Hz, 1000 Hz [G.R.8]..

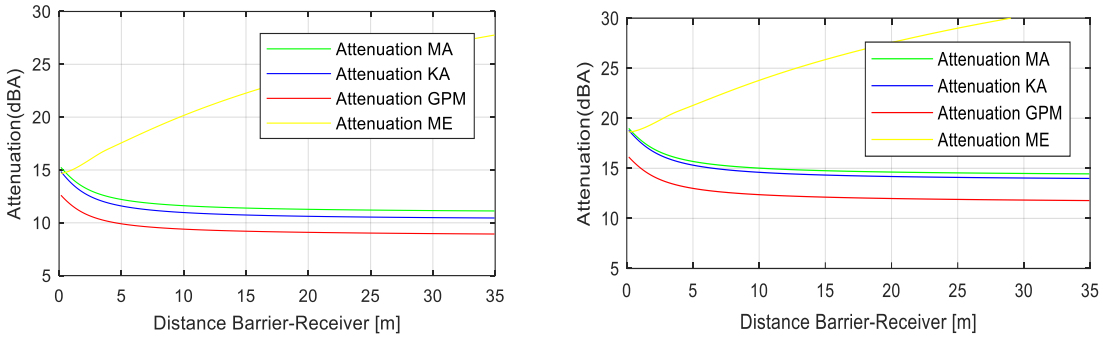

a. Frequency = 100 Hz b. Frequency = 250 Hz

Fig.4.3. Sound attenuation as a function of the distance barrier-receiver and for a pure tone at 100 Hz(a) and at 250 Hz(b).[G.R.8, G.R.22]

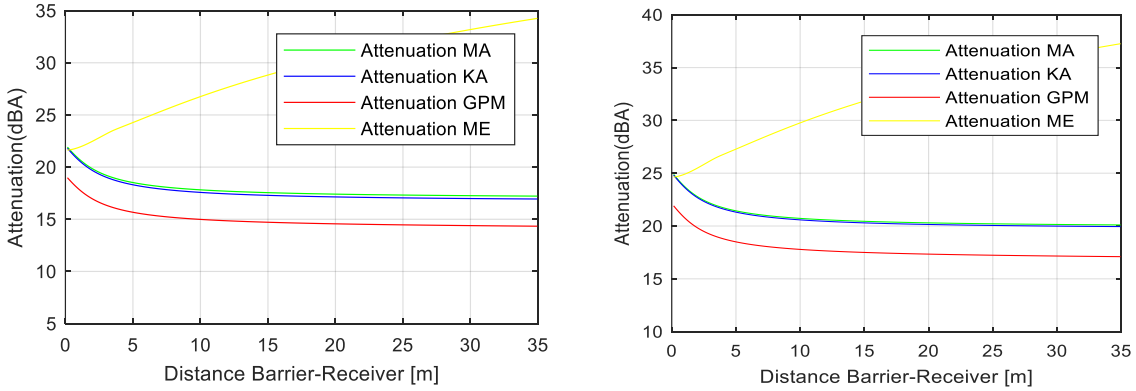

a. Frequency = 500 Hz b. Frequency = 1000 Hz

Fig. 4.4. Sound attenuation as function of the distance barrier-receiver and for a pure tone. [G.R.8, G.R.22]

In Figure 4.5 a. is represented the sound attenuation for all four methods at the sound frequency of 2000 Hz but separately it represents the attenuation due to spherical wave propagation (SWE in Figure 4.5.a.) and from attenuation given by Menounou it was subtracted the attenuation due to spherical wave propagation (SWE). Figure 4.5.b presents the attenuation due only to spherical wave propagation (SWE-spherical wave effect) therefore it can be seen now that the attenuation due to spherical wave propagation (SWE) introduces the "over attenuation" in the Menounou

approach, therefore, the last term in equation (4.10), the term given by relation (4.14), will be put to zero starting from this point forward for the attenuation given by Menounou approach.

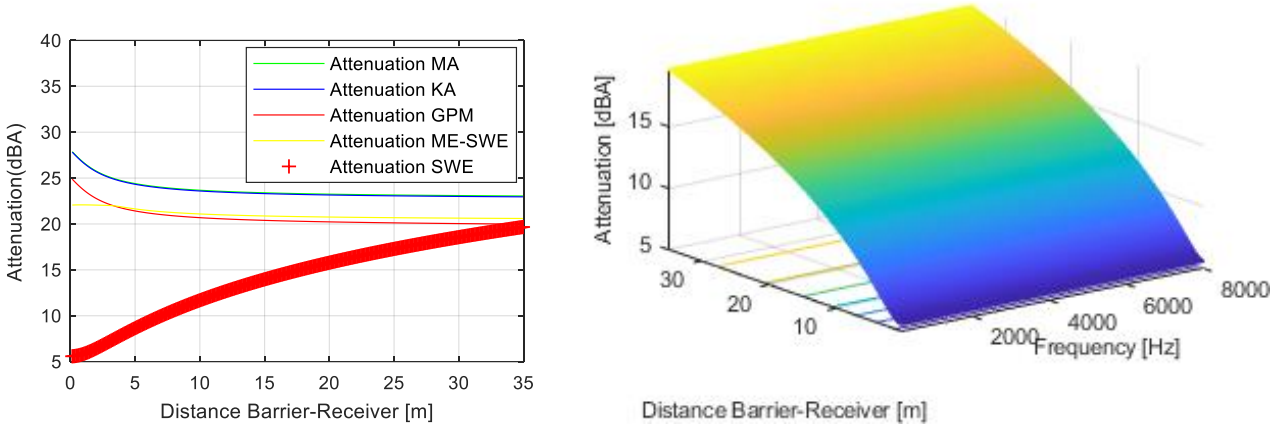

a. Frequency = 2000 Hz. b. Attenuation due to SWE. Range frequency 100 Hz-8000 Hz.

Fig. 4.5. Sound attenuation as function of the distance barrier-receiver and for a pure tone. [G.R.8, G.R.22]

In figures 4.6 a. and 4.6 b. it were considered the effect of ground (ground absorption as well as ground reflections), given by equations (4.16) and (4.17), as well as air absorption given by relations (4.18) and (4.19) for a relative humidity of the air of 20%, for two values of effective flow resistivity of the ground σ_e = 10 MPa s m-2 and σ_e = 104 kPa s m^{-2} and the sound frequency of 1000 Hz for all the four approaches: Maekawa-Tatge approach, Kurze-Anderson algorithm, GPM, Menounou -SWE formulation. It means that all the methods are modified by these two effects: ground absorption-reflections and air humidity (in figures it was marked as MMA-Modified Maekawa, MKA-Modified Kurze&Anderson, MGPM- Modified GPM, MME-Modified Menounou) [G.R.8].

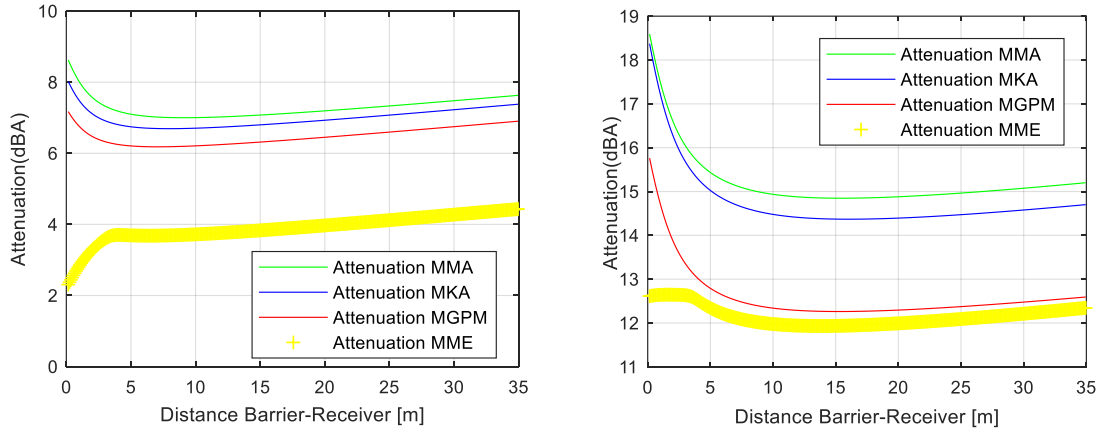

a. Relative humidity: 20%; σ_e = 10 MPa·s·m^{-2}. b. Relative humidity: 20%; σ_e = 104 kPa·s·m^{-2}.

Fig. 4.6. Sound attenuation as a function of the distance barrier-receiver and for a pure tone at 1000 Hz. [G.R.8, G.R.22]

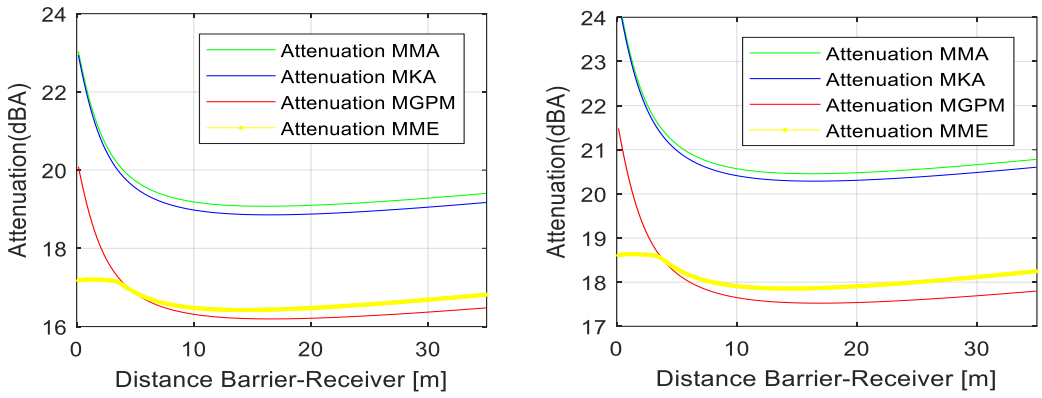

a. Frequency = 2000 Hz. b. Frequency = 2500 Hz.

Fig. 4.7. Sound attenuation as function of the distance barrier-receiver and for a pure tone: σe= 104 kPa·s·m-2. [G.R.8, G.R.22]

Comparing the results from figure 7 a. with the experimental data in the literature [R.C.4.10, G.R.16] (p. 361 global experimental data in graphs) the method that is in close agreement with data published is MGPM. Taking into consideration all the aspects mentioned before, the proposed predicted noise attenuation MGPM is given by the equation:

$$A_{MGPM} = 10\log_{10}\left(3+20N_1^{'}\right)+\left[6\tanh\sqrt{N_2}-2-20\log_{10}\left[1+\tanh\left(0.6\log_{10}\frac{N_2}{N_1}\right)\right]\right] \quad (4.28)$$

$$\left[1-\tanh\sqrt{10N_1}\right]+\alpha_{aa}\left(r_1+r_2\right)$$

One of the most used "head edge" semi-infinite noise barrier is the Y-shape, presented in Figure 4.9 because by varying the Y-angle α from 0^0 to 180^0 the Y-shape is transformed into a T-shape and the β angle of the direction for the symmetry line of Y-shape can be modified in the range 0^0 to 180^0 with respect to the ground horizontal line, as presented in the literature [G.R.16]. Using the MGPM (Modified General Prediction Method) to compute the attenuation of the sound with a semi-infinite thin rigid barrier for the same geometrical conditions as presented above it was optimized the Y-shape of the diffracting edge considering a = 0.2 m, h = 0.5 m mounted in point E (see Figures 4.1 and 4.9). Figures 4.10 and 4.11 are presented the numerical results for a distance barrier-receiver of 35 m and for three frequencies of the pure tone sound 1000 Hz, 2000 Hz, and 4000 Hz, and considering that the relative air humidity is 20% and the effective flow resistivity of the ground is σ_e= 104 kPa·s·m^{-2}. As can be seen from Figures 4.10 and 4.11 the optimal angles of the Y-shape diffraction edge that induces the maximum sound attenuation of the barrier, computed with MGPM, are α= 179^0 (almost T-shape) and β = 72^0, β being the angle of inclination with respect to the ground horizontal towards the source S, that is in close agreement with the experimental results presented in literature [G.R.16] (α= 180^0 T shape (p. 366), β = 70^0 (p. 366)). In this way, the MGPM is tested to predict the noise attenuation closer to the reality phenomena than GPM. We can conclude that the best method to predict the sound attenuation of a noise with a semi-infinite thin rigid barrier is the Modified General Prediction Method (based on ISO 9613-2) that takes into consideration the next effects: diffraction effect of the edge barrier based on Fresnel number N_1 (basic for GPM and SoundPLAN), the downwind meteorological effects that modifies the Fresnel number N_1 (basic for GPM and SoundPLAN), the effect of the proximity of the receiver to the shadow boundary involving the both modified Fresnel numbers N_1 and N_2 (novelty with respect to GPM and SoundPLAN), the effect of sound air relative humidity absorption based on ISO 9613-1 (novelty with respect to GPM and SoundPLAN) and the combined effects of absorption- reflections of the ground

(novelty with respect to GPM and SoundPLAN), using an algorithm containing the relations: (4.1),(4.2),(4.7),(4.8),(4.14) and (4.16) - (4.20).

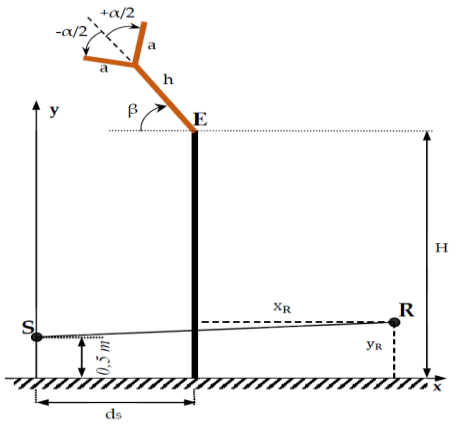

Fig.4.9. The Y-shape of the "head edge" for the semi-infinite noise barrier.[G.R.19]

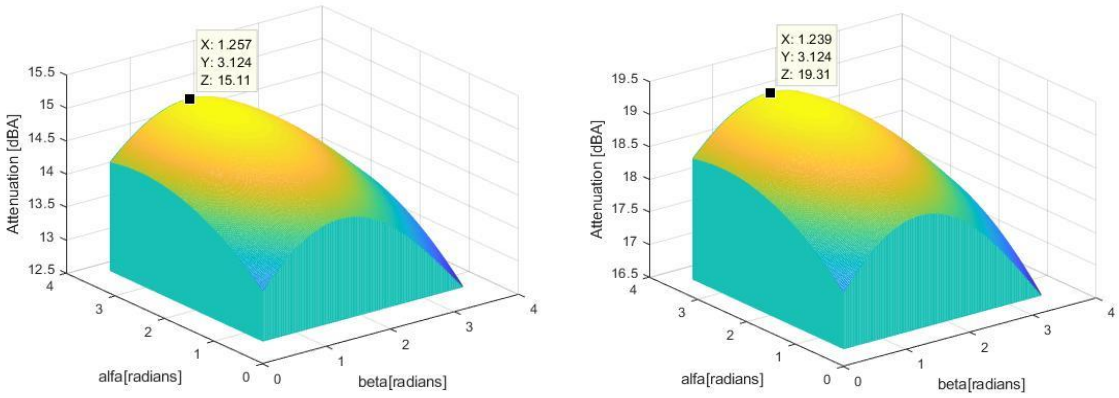

a. frequency = 1000 Hz. b. frequency = 4000 Hz.

Fig. 4.10. Sound Attenuation: Distance barrier-receiver 35 m; Relative air humidity 20%; σ_e= 104 kPa·s·m^{-2}. [G.R.19]

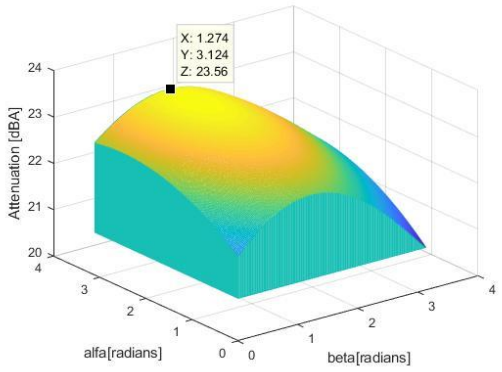

Fig. 4.11**.** Sound Attenuation: Distance barrier-receiver 35 m; Sound frequency =4000 Hz; Relative humidity 20%; σ_e= 104 kPa·s·m^{-2}. [G.R.19]

Chapter 5. Optimization of asymmetric edge diffraction on the top of acoustic barriers for industrial and automotive/railway traffic noise attenuation

5.1.Introduction

The present chapter presents a detailed optimization of specific edge diffraction (asymmetric edge diffraction) mounted on an acoustic barrier using the Modified General Prediction Method (MGPM)[G.R.8]. The computation of the noise attenuation using acoustic barriers is enhanced by considering four different approaches: Maekawa-Tatge formulation, Kurze - Anderson algorithm, and general prediction method (GPM-ISO 9613), and Menounou formulation. The noise attenuation of the barrier was computed based on the Kirchhoff diffraction theory, which implies that the Huygens-Fresnel theory is applied to a semi-infinite acoustic thin barrier. The Maekawa-Tatge formulation and Kurze and Anderson algorithm provide almost the same numerical results since they express the noise attenuation using the first Fresnel number N_1. This indicates that only one phenomenon is considered: The effect of the relative position of the receiver from the source. For the prediction of noise attenuation, the general prediction method considers two phenomena: the effect of the relative position of the receiver from the source and the downwind meteorological effect. The Menounou formulation takes into consideration four phenomena: The effect of the relative position of the receiver from the source, the effect of the proximity of the source or the receiver to the midplane, the effect of the proximity of the receiver to the shadow boundary, and the diffraction effect due to spherical incident waves.

The best-predicting method for the computation of the noise attenuation for a thin, rigid, semi-infinite acoustic barrier is MGPM. The MGPM is an improvement of GPM by introducing new effects, such as the proximity of the source or the receiver to the midplane attenuation due to geometrical divergence, ground absorption-reflections, and atmospheric absorption. The MGPM was tested as mentioned in [G.R.8], and close agreements with data in the literature were found [G.R.16]. This research aimed to provide an optimization using MGPM for specific edge diffraction mounted on a thin, rigid acoustic barrier in an industrial area[G.R.23].

5.2. Optimization of asymmetric edge diffraction on the top of acoustic barriers for industrial areas noise attenuation

For the optimization of asymmetric edge diffraction on the top of acoustic barriers for industrial areas noise attenuation it were used the relations:

$$k = \frac{\omega}{c} = \frac{2\pi f}{c}, \tag{5.1}$$

$$k_{\text{mod}} = \frac{k}{|\alpha_{gr}|}, \tag{5.2}$$

$$\alpha_{gr} = 1 + 0.0978\left(\frac{f}{\sigma_e}\right)^{-0.7} - i0.189\left(\frac{f}{\sigma_e}\right)^{-0.595}, i = \sqrt{-1} \tag{5.3}$$

$$N_1 = \frac{2\delta_1 f}{c} = \frac{k_{\text{mod}}}{\pi}\delta_1, N_2 = \frac{2\delta_2 f}{c} = \frac{k}{\pi}\delta_2 \tag{5.4}$$

$$\delta_1 = r_1 + r_2 - \sqrt{\left(d_s + x_R\right)^2 + \left(y_R - 0{,}5\right)^2} = r_1 + r_2 - d_1$$

$$\delta_2 = r_1 + r_2 - \sqrt{\left(x_R - d_s\right)^2 + \left(y_R - 0{,}5\right)^2} = r_1 + r_2 - d_2 \tag{5.5}$$

$$K_{met} = e^{-\frac{1}{2000}\sqrt{\frac{r_1 r_2 d_2}{2\delta_1}}} \quad N_1^{'} = 0.5 N_1 K_{met} \tag{5.6}$$

$$\alpha_{aa} = f^2 \left[\left(\frac{1.84x10^{-11}}{\left(\frac{T_O}{T}\right)^{0.5} \frac{p_S}{p_O}} \right) + \left(\frac{T_O}{T}\right)^{2.5} \left(\frac{0.10680e^{-3352/T} f_{r,N}}{f^2 + f_{r,N}^2} + \frac{0.01278e^{-2239.1/T} {}_{fr,O}}{f^2 + f_{r,O}^2} \right) \right] \tag{5.7}$$

$$A_{MGPM} = 10\log_{10}\left(3 + 20N_1^{'}\right) + \left[6\tanh\sqrt{N_2} - 2 - 20\log_{10}\left[1 + \tanh\left(0.6\log_{10}\frac{N_2}{N_1} \right) \right] \right] \cdot$$

$$\cdot \left[1 - \tanh\sqrt{10N_1} \right] + \alpha_{aa}\left(r_1 + r_2\right), \tag{5.8}$$

where the signification of the terms in (5.1) – (5.8) is the same as in Chapter 4.

Figure 5.2 is illustrated specific edge diffraction mounted on the top of an infinitely thin, rigid acoustic barrier designed for noise attenuation in an industrial area. The geometrical data characteristics of the edge and the infinite thin, rigid acoustic barrier are mentioned in table 5.1, while the angles α, β, and γ are variable and need to be optimized.

H[m]	h[m]	x_R[m]	y_R[m]	d_S[m]	a[m]		b[m]
4	0.2	0.5…30	1.7	10	0.30		0.60

Table 5.1. Geometrical details of the edge and the infinite thin, rigid acoustic barrier [G.R.19].

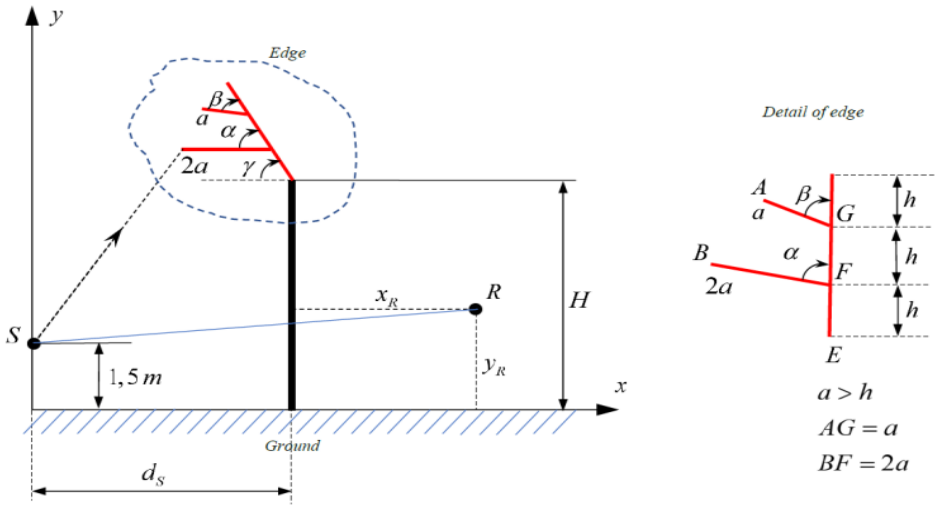

Fig.5.2. Specific(asymmetric) edge on the top of the acoustic barrier. [G.R.19]

Figures 5.3-5.14 illustrate the noise attenuation for this specific edge mounted on an infinite thin rigid barrier(see Figure 5.2), having a height H = 4m in an industrial area, considering the source placed at d_S=10m at a height y_S=1.5m and the geometry of the edge presented in table 5.1. It was considered a distance barrier-receiver of 30 m, and for two frequencies of the pure tone sound at 1000Hz and 4000 Hz, are presented in Figures 5.3-5.14 the noise attenuation. In addition, the following factors were considered: the relative air humidity is 20%, and the effective flow resistivity of the ground is σ_e = 104 kPa·s·m^{-2}. The angles are in the range $\alpha = 1^0 \ldots 180^0$, $\beta = 1^0 \ldots 180^0$, $\gamma = -85^0 \ldots +85^0$.

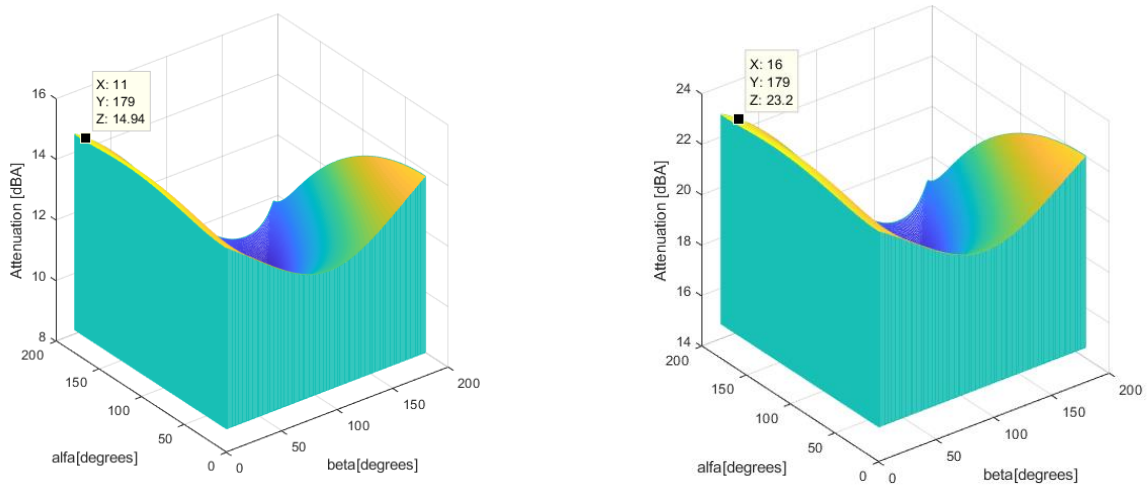

(a) Frequency = 1000 Hz (b) frequency = 4000 Hz

Fig. 5.3. Sound attenuation: Distance barrier-receiver 30 m; relative air humidity 20%; σ_e= 104 kPa·s·m^{-2}, γ=-85^0. [G.R.19]

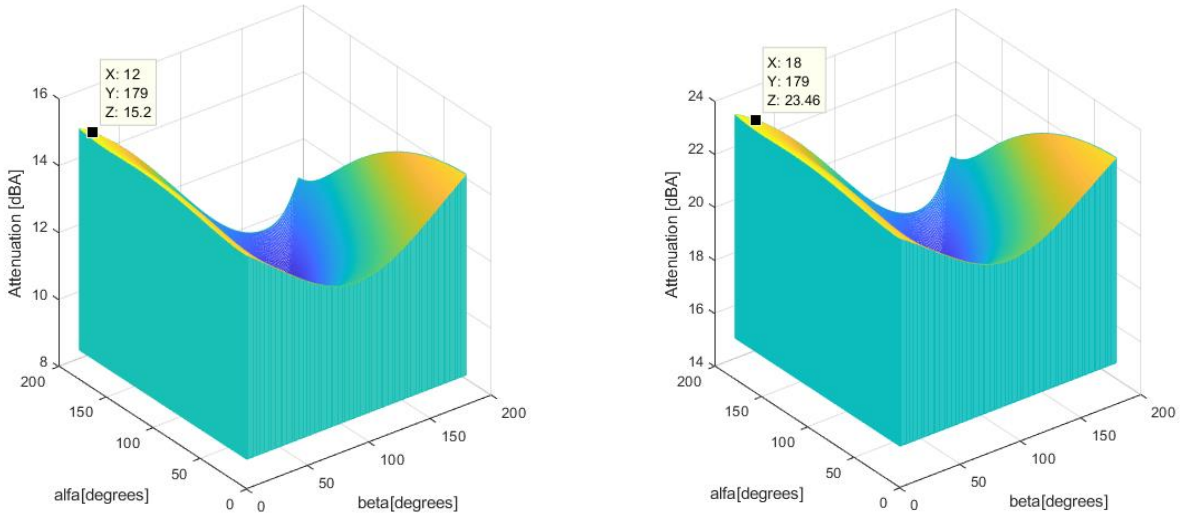

(a) Frequency = 1000 Hz (b) frequency = 4000 Hz

Fig. 5.4. Sound attenuation: Distance barrier-receiver 30 m; relative air humidity 20%; σ_e= 104 kPa·s·m^{-2}, γ=-70^0. [G.R.19]

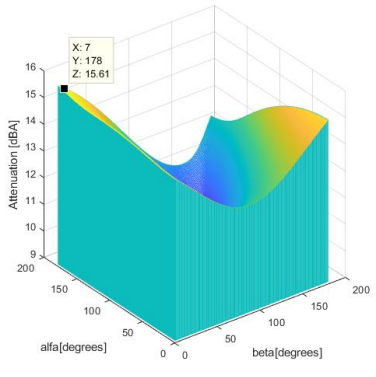

(a) Frequency = 1000 Hz

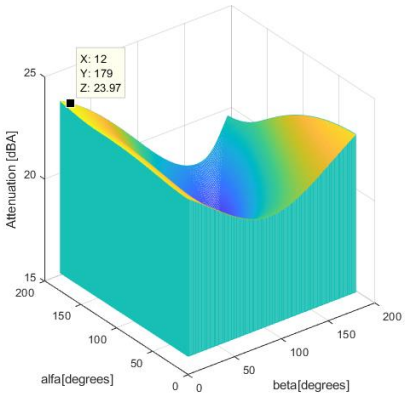

(b) frequency = 4000 Hz

Fig. 5.5. Sound attenuation: Distance barrier-receiver 30 m; relative air humidity 20%; σ_e= 104 kPa·s·m^{-2}, γ=-55^0. [G.R.19]

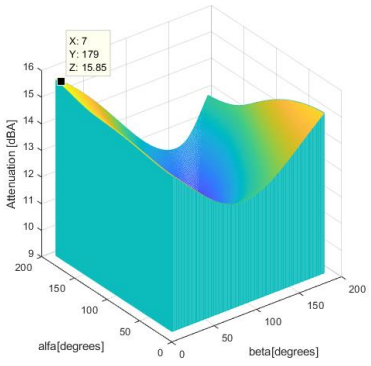

(a) Frequency = 1000 Hz

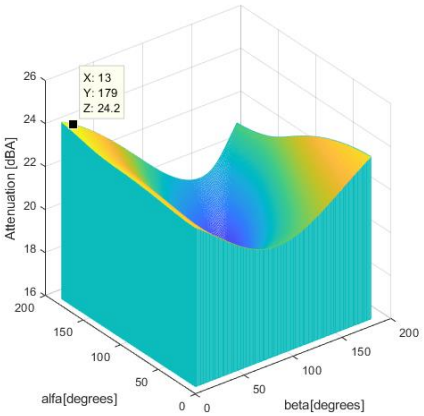

(b) frequency = 4000 Hz

Fig. 5.6. Sound attenuation: Distance barrier-receiver 30 m; relative air humidity 20%; σ_e= 104 kPa·s·m^{-2}, γ=-40^0. [G.R.19]

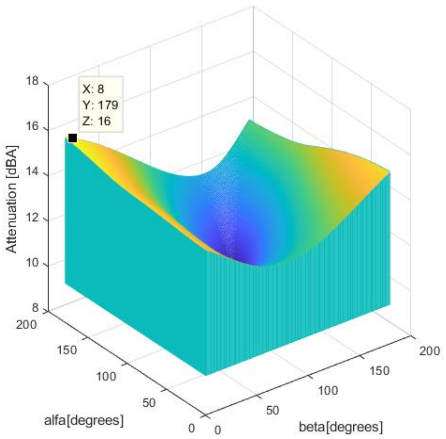

(a) Frequency = 1000 Hz

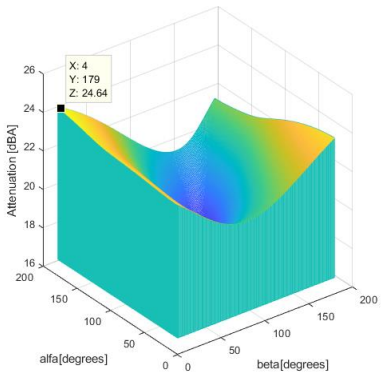

(b) frequency = 4000 Hz

Fig. 5.7. Sound attenuation: Distance barrier-receiver 30 m; relative air humidity 20%; σ_e= 104 kPa·s·m^{-2}, γ=-25^0. [G.R.19]

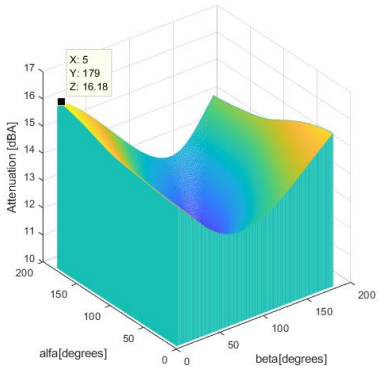

(a) Frequency = 1000 Hz

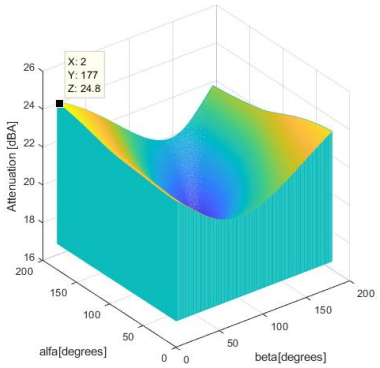

(b) frequency = 4000 Hz

Fig. 5.8. Sound attenuation: Distance barrier-receiver 30 m; relative air humidity 20%; σ_e= 104 kPa·s·m^{-2}, γ =-10^0. [G.R.19]

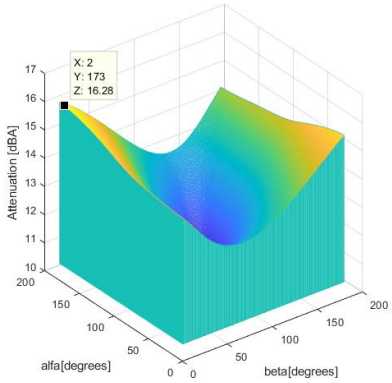

(a) Frequency = 1000 Hz

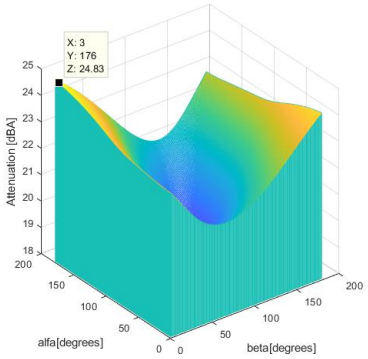

(b) frequency = 4000 Hz

Fig. 5.9. Sound attenuation: Distance barrier-receiver 30 m; relative air humidity 20%; σ_e= 104 kPa·s·m^{-2}, γ=10^0. [G.R.19]

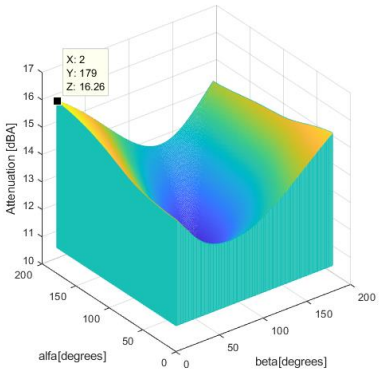

(a) Frequency = 1000 Hz

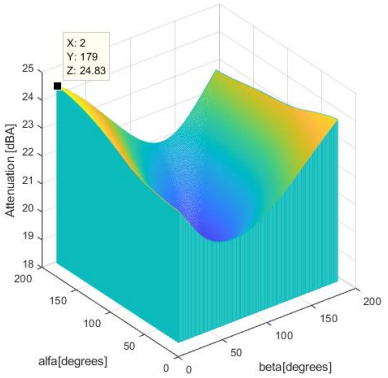

(b) frequency = 4000 Hz

Fig. 5.10. Sound attenuation: Distance barrier-receiver 30 m; relative air humidity 20%; σ_e= 104 kPa·s·m^{-2}, γ=25^0.

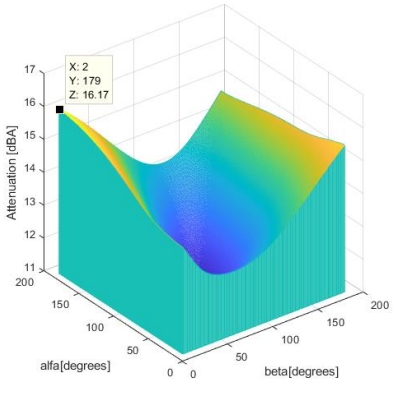

(a) Frequency = 1000 Hz

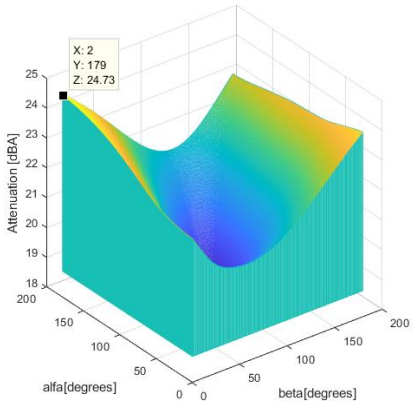

(b) frequency = 4000 Hz

Fig. 5.11. Sound attenuation: Distance barrier-receiver 30 m; relative air humidity 20%; σ_e= 104 kPa·s·m^{-2}, γ=40^0. [G.R.19]

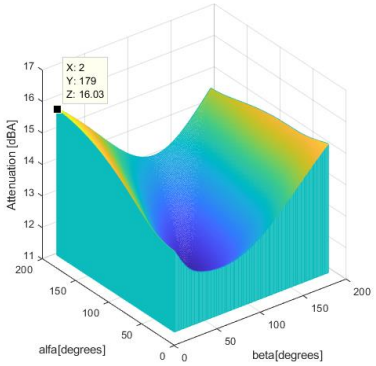

(a) Frequency = 1000 Hz

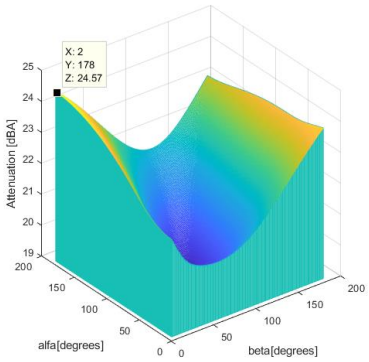

(b) frequency = 4000 Hz

Fig. 5.12. Sound attenuation: Distance barrier-receiver 30 m; relative air humidity 20%; σ_e= 104 kPa·s·m^{-2}, γ=55^0. [G.R.19]

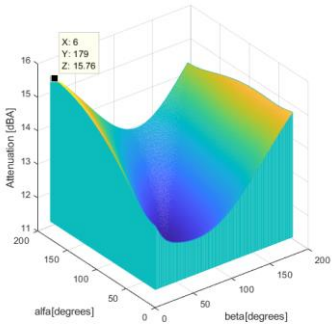

(a) Frequency = 1000 Hz

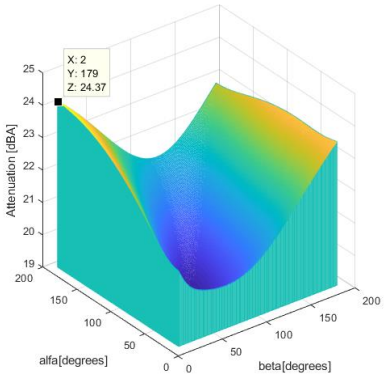

(b) frequency = 4000 Hz

Fig. 5.13. Sound attenuation: Distance barrier-receiver 30 m; relative air humidity 20%; σ_e= 104 kPa·s·m^{-2}, γ=70^0. [G.R.19]

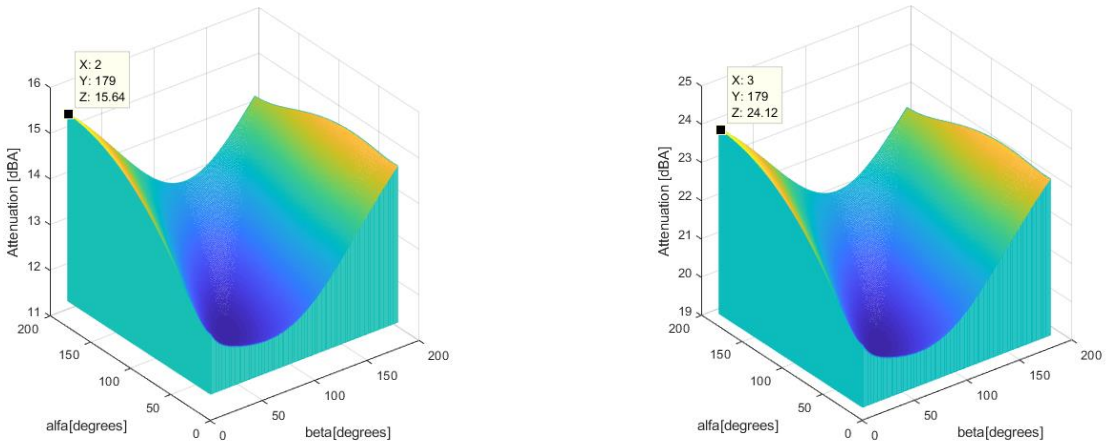

(a) Frequency = 1000 Hz (b) frequency = 4000 Hz

Figure 5.14. Sound attenuation: Distance barrier-receiver 30 m; relative air humidity 20%; σ_e= 104 kPa·s·m^{-2}, γ=85^0.[G.R.19]

Analyzing the graphs presented in Figures 5.3 – 5.14 it can be remarked that the best attenuation for both frequencies of pure noise 1 kHz and 4 kHz is obtained for $\alpha = 179^0$, $\beta = 2^0$, and $\gamma=85^0$ considering that a = 0.3m and b = 0.6m. The results are in close agreement with data in the literature [G.R.3; G.R..4]. The investigation certifies that the MGPM is also an appropriate method to predict noise attenuation in the industrial area using acoustic barriers with specific edge diffraction as it is a suitable method that predicts noise attenuation for automotive highway traffic using acoustic barriers. The optimization of edge diffraction for acoustic barriers is very useful in the design stage of such acoustical devices. [G.R.19]

5.3 Optimization of asymmetric edge diffraction on the top of acoustic barriers for automotive/railway traffic noise attenuation.

The present paragraph presents a detailed investigation of asymmetric edge diffraction mounted on a rigid acoustic barrier designed for automotive and railway traffic noise attenuation. The study comprises the optimization of the asymmetric edge diffraction using the Modified General Prediction Method (MGPM) developed by the authors in previous research[G.R.23]. The MGPM can be applied directly for symmetric edge diffraction (previous Chapter) but must be modified for asymmetric edge diffraction. In general, asymmetric edge diffraction is used for attenuating industrial noise, as mentioned by Okubo and Fujiwara in [R.C.5.1], but the author of the paragraph analysis also the possibilities of using such types of edge diffraction for automotive and railway traffic noise attenuation(AARTNA). The noise attenuation of the barrier, enhancing the MGPM, is computed based on the Kirchhoff diffraction theory, which implies that the Huygens-Fresnel theory is applied to a semi-infinite acoustic thin, rigid barrier (SIATRB). This research aimed to provide a modified version of MGPM for asymmetric edge diffraction (AED) mounted on an SIATRB designed for AARTNA.

Figure 5.15 illustrates an SIATRB with the height H, an acoustic source (AS) with the coordinates $(0, y_S)$, an acoustic receiver (AR) with the coordinates $(x_R + x_S, y_R)$, and an AED with the geometry details.

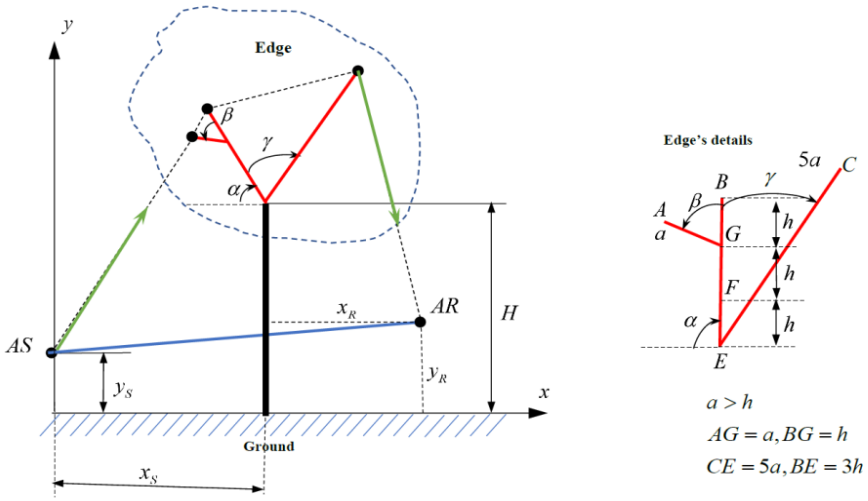

Fig. 5.15. An SIATRB with an AED mounted on the top. [G.R.24]

The MGPM considers the attenuation introduced by ground absorption reflections, and for this, the most convenient model is the Delany-Bazley model [G.R.13], resulting in the modified wavenumber k_{mod} due to "*the effect of ground absorption*"[G.R.8].

$$K_{\text{mod}} = \frac{2\pi}{c\left[1+0.0978\left[\frac{f}{\sigma_e}\right]^{-0.7} - i0.189\left[\frac{l}{\sqrt{e}}\right]^{-0.595}\right]}, i = \sqrt{-1} \tag{5.9}$$

where f is "*the pure tone frequency*"(PTF)[G.R.8], σ_e is "*the effective flow resistivity of the ground*"(EFRG)[G.R.8; G.R.13], and c is "*the sound speed in the air*"(SSA)[G.R.8]. Based on the Kirchhoff-Fresnel diffraction theory [G.R.7](pp. 113–147), the Fresnel numbers of the AS and the image of the AS, respectively AS' (the symmetric geometric point concerning the plane of the barrier) are N_1, N_2, given by the relations [G.R.23]

$$N_1 = \frac{2\delta_1 f}{C} = \frac{k_{1\text{mod}}}{\pi}\delta_1, N_2 = \frac{2\delta_2 f}{C} = \frac{k_{1\text{mod}}}{\pi}\delta_2 \tag{5.10}$$

where δ_1, δ_2 are the distances defined by the longest propagation way of the acoustic wave and the shortest one, respectively (AS $\rightarrow$A $\rightarrow$B $\rightarrow$C $\rightarrow$AR) - (AS $\rightarrow$AR), and (AS $\rightarrow$A $\rightarrow$B $\rightarrow$C $\rightarrow$ AR) - (AS' $\rightarrow$AR), defined by the expressions:

$$\delta_1 = r_1 + r_2 + r_3 + r_4 - \sqrt{\left(x_S + x_R\right)^2 + \left(y_R - y_S\right)^2} = r_1 + r_2 + r_3 + r_4 - d_1,$$

$$
\begin{aligned}
&r_1=\sqrt{\left(0-x_A\right)^2+\left(y_S-y_A\right)^2}, r_2=\sqrt{\left(x_B-x_A\right)^2+\left(y_B-y_A\right)^2},\\
&r_3=\sqrt{\left(x_C-x_B\right)^2+\left(y_C-y_B\right)^2}, r_4=\sqrt{\left(x_R+x_S-x_C\right)^2+\left(y_R-y_C\right)^2},\\
&x_A=x_S-2h\cos\alpha-a\cos\left(\alpha-\beta\right)=a\left(x_S/a-2\varsigma\cos\alpha-\cos\left(\alpha-\beta\right)\right), \varsigma=h/a, \varsigma=0.5-0.9,\\
&y_A=H+2h\sin\alpha+a\sin\left(\alpha-\beta\right)=a\left(H/a+2\varsigma\sin\alpha+\sin\left(\alpha-\beta\right)\right),\\
&x_B=x_S-3h\cos\alpha=a\left(x_S/a-3\varsigma\cos\alpha\right), y_B=H+3h\sin\alpha=a\left(H/a+3\varsigma\sin\alpha\right),\\
&x_C=xS-5a\cos\left(\alpha+\gamma\right)=a\left(x_S/a-5\cos\left(\alpha+\gamma\right)\right), y_B=H+5a\sin\left(\alpha+\gamma\right)=a\left(H/a+5\sin\left(\alpha+\gamma\right)\right),
\end{aligned}
\tag{5.11}
$$

$$
\delta_2=r_1+r_2+r_3+r_4-\sqrt{\left(x_R-x_S\right)^2+\left(y_R-y_S\right)^2}=r_1+r_2+r_3+r_4-d_2, x_R>x_S, y_R>y_S
$$

where d_1 is the distance between the points AS and AR(respectively (AS $\rightarrow$ AR)), while d_2 is the distance between the points AS' and AR(respectively (AS' $\rightarrow$ AR)). Because the GPM [G.R.10; G.R.11] provides a relation for the sound attenuation based on a modified Fresnel number $N_1^{'}$ as mentioned in ISO 9613-2 [G.R.17], taking into consideration a correction factor for the downwind meteorological effect *Kmet*, the MGPM considers the same correction factor thus, yielding the relations[G.R.24]:

$$
K_{met}=\exp\left(-\frac{1}{2000}\sqrt[4]{\frac{r_1r_2r_3r_4d_1}{2\delta_1}}\right), N_1^{'}=0.5N_1K_{met} \tag{5.12}
$$

The MGPM also considers(see [G.R.23]) the AA using the Larsson model [G.R.14], which induces in the predictive model the following effects: sound frequency, air humidity, air temperature, and pressure, using an attenuation coefficient α_{aa}, expressed in dBA/m, described by the relation [G.R.23]:

$$
K_{met}=f^2\left[\left(\frac{1.84x10^{-11}}{\left(\frac{T_0}{T}\right)^{0.5}\frac{p_s}{p_0}}\right)+\left(\frac{T_0}{T}\right)^{2.5}\left(\frac{0.1068e^{-3352/T}f_{r,N}}{f^2+f_{r,N}^2}+\frac{0.01278e^{-2239.1/T}f_{r,O}}{f^2+f_{r,O}^2}\right)\right] \tag{5.13}
$$

where the significations of the terms are explained in detail in [G.R.14, G.R.15]. Considering all the aspects mentioned above, expressed by the relations (5.9)-(5.13), the sound attenuation proposed by MGPM [G.R.8] when using an SIATRB for AARTNA with an AED is given by the equation

$$
\begin{aligned}
&A_{MGPM}=10\log_{10}(3+20N_1^{'})+\alpha_{aa}(r_1+r_2+r_3+r_4)+\\
&+\left[6\tanh\sqrt{N_2}-2-20\log_{10}\left[1+\tan g\left(0.6\log_{10}\frac{N_2}{N_1^{'}}\right)\right]\right]\left[1-\tanh\sqrt{10N_1^{'}}\right].
\end{aligned}
\tag{5.14}
$$

To have the diffractions directions that induce the sound attenuation in conformity with the mathematical algorithm generated by the expressions (5.9)-(5.14), it is necessary to impose certain simultaneous geometrical restrictions as follows

1. point A must be "over" the direction line $AS \rightarrow B$,
2. point C must be "over" the direction line $B \rightarrow AR$,
3. $h < a, h / a = \varsigma \in [0.5, 0.9]$.

Condition 2, for an existing condition three true, is satisfied if:

$$\alpha + \gamma \leq \pi \tag{5.15}$$

while condition 1 is satisfied for

$$\beta \leq \beta \max = \pi - \phi - \arcsin(\varsigma \sin\phi)\phi = arcc\,os\left[\frac{x_B^2 + (y_b - y_s)^2 + 9(a\varsigma)^2 - x_S^2 - (H - y_s)^2}{6a\varsigma\sqrt{x_B^2 + (y_B + y_S)^2}}\right] \tag{5.16}$$

Condition 3, together with relations (5.15) - (5.16) and the expressions of the coordinates, $x_A, y_A, x_B, y_B, x_C, y_C$ define from a geometrical point of view the existence of an asymmetric edge diffraction(AED) for an SIATRB designed to obtain a convenient AARTNA. The aspects mentioned before are valid for the angles α, β, γ satisfying the conditions [G.R.24]

$$\alpha \in \left[1^0, 179^0 - \phi_1\right], \phi_1 = arctg\frac{H - y_s}{x_s}, \tag{5.17}$$

$$\beta \in \left[1^0, \beta_{\max}\right], \beta_{\max} \Leftarrow (8) \tag{5.18}$$

$$\gamma \in \left[1^0 \gamma_{\max}\right], \gamma_{\max} = 1^0 + arctg\frac{H - y_s}{x_s} \tag{5.19}$$

and the attenuation is computed using the algorithm given by equations (5.9)-(5.14), representing the first part of the investigation. The second part of the investigation the angles α, β, γ satisfy the conditions

$$\alpha \in \left[180^0 - \phi_1, 179^0\right], \phi_1 = arctg\frac{H - y_s}{x_s}, \tag{5.20}$$

$$\beta \in \left[1^0, 179^0\right], \tag{5.21}$$

$$\gamma \in \left[1^0, arctg\frac{H - y_s}{x_s}\right], \tag{5.22}$$

but the attenuation is computed in this case by modifying equations (5.11) and (5.12) due to modifications of the propagation way for the acoustic wave that are ($AS \rightarrow E \rightarrow A \rightarrow B \rightarrow C \rightarrow AR$)-($AS \rightarrow AR$), respectively ($AS \rightarrow E \rightarrow A \rightarrow B \rightarrow C \rightarrow AR$) - ($AS' \rightarrow AR$), defined by the relations [R.G.24]

$$\delta_1 = r_1 + r_2 + r_3 + r_4 + r_5 - \sqrt{(x_S + y_R)^2 + (y_R - y_S)^2} = r_1 + r_2 + r_3 + r_4 + r_5 - d_{1'}$$

$$r_1 = \sqrt{(x_S)^2 + (H - y_S)^2}, r_2 = \sqrt{(x_A - x_S)^2 + (y_A - H + y_S)^2}, r_3 = \sqrt{(x_B - x_A)^2 + (y_B - y_A)^2}$$
$$r_4 = \sqrt{(x_C - x_B)^2 + (y_C - y_B)^2}, r_5 = \sqrt{(x_R + x_S - x_C)^2 + (y_R - y_C)^2},$$

$$x_A = x_S - 2h\cos\alpha - a\cos(\alpha - \beta) = a(x_S / a - 2\varsigma\cos\alpha - \cos(\alpha - \beta)), \varsigma = h / a, \varsigma = 0.5 - 0.9$$

$$y_A = H + 2h\sin\alpha + a\sin(\alpha - \beta) = a(H / a + 2\varsigma\sin\alpha + \sin(\alpha - \beta)) \quad (5.23)$$

$$x_B = x_S - 3h\cos\alpha = a(x_S / a - 3\varsigma\cos\alpha), y_B = H + 3h\sin\alpha = a(H / a + 3\varsigma\sin\alpha)$$

$$x_C = x_S - 5a\cos(\alpha + \gamma) = a(x_S / a - 5\cos(\alpha + \gamma)), y_B = H + 5a\sin(\alpha + \gamma) = a(H / a + 5\sin(\alpha + \gamma))$$

$$\delta_2 = r_1 + r_2 + r_3 + r_4 + r_5 - \sqrt{(x_R + x_s)^2 + (y_R - y_S)^2} = r_1 + r_2 + r_3 + r_4 + r_5 - d_{2'}$$

and the modified Fresnel number $N_1^{'}$, as mentioned in ISO 9613-2 [R.G.17], taking into consideration the correction factor for the downwind meteorological effect *Kmet* , is defined by the equations [R.G.24]:

$$K_{met} = \exp\left(-\frac{1}{2000}\sqrt[5]{\frac{r_1 r_2 r_3 r_4 r_5 d_1}{2\delta_1}}\right), N_1^{'} = 0.5 N_1 K_{met} \quad (5.24)$$

In this second case, the sound attenuation proposed by MGPM [R.G.8] when using an SIATRB for AARTNA with an AED is given by the equation [R.G.24]:

$$A_{MGPM} = 10\log_{10}(3 + 20N_1^{'}) + \alpha_{aa}(r_1 + r_2 + r_3 + r_4 + r_5) +$$
$$+\left[6\tanh\sqrt{N_2} - 2 - 20\log_{10}\left[1 + \tanh\left(0.6\log_{10}\frac{N_2}{N_1^{'}}\right)\right]\right]\left[1 - \tanh\sqrt{10N_1^{'}}\right] \quad (5.25)$$

where $N_1^{'}$ is determined using equations (5.9), (5.10), (5.23), (5.24), and for the last equation, in addition, is used equation (5). It can be concluded that the mathematical algorithm in the second case to compute the AARTNA using an SIATRB with an AED is given by the equations (5.9), (5.10), (5.13), (5.23)-(5.25). Figure 5.15 illustrates an AED mounted on the top of the SIATRB designed for AARTNA, and the geometrical data characteristics of the AED and the SIATRB are mentioned in Table 5.2, while the angles α, β, and γ are variable and need to be optimized [G.R.2].

Tabel 5.2. Geometrical details of the AED and the SIATRB

H[m]	x_S [m]	y_S [m]	x_R [m]	y_R [m]	a[m]	ς =h/a
4	3.0	0.4	2...50	1.5	0.20	0.5....0.9

Using equations (5.9)-(5.14), for the first case defined by the conditions (5.17 - 5.19), and the equations (5.9), (5.10), (5.13),(5.23)-(5.25), for the second case defined by the conditions (5.20 – 5.22), it was developed MATLAB software to calculate the AARTNA for the SIATRB with AED. Figures 5.16-5.19 illustrate the noise attenuation for the first case considering $x_R = 25.0$ m, the sound's PTF $f = 1.0$ kHz, the EFRG $\sigma_e = 1.0 \cdot 10^5$ Pa·s·m^{-2}, $\varsigma = 0.5, 0.9$ and the angles range $\alpha \in \left[1^0, 129^0\right], \gamma \in \left[1^0, 51^0\right], \beta \in \left[1^0, \beta_{max}\right]$ (for β_{max} see (5.8)).

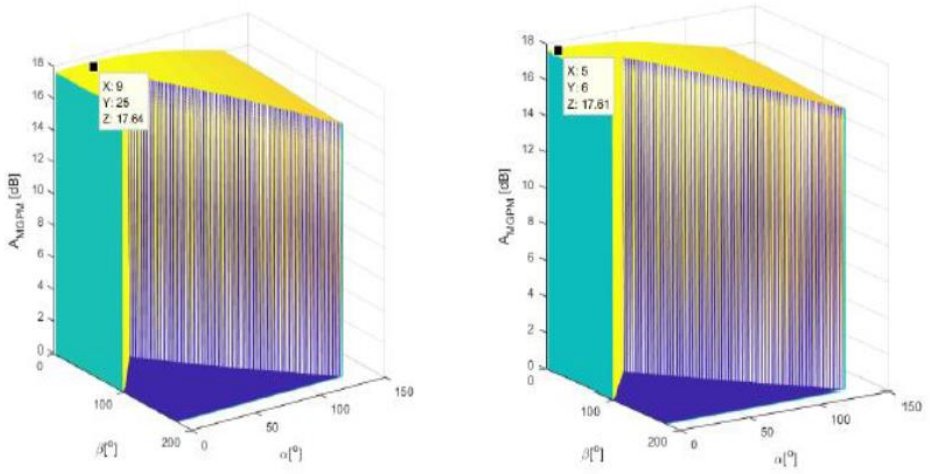

a) b)

Fig..5. 16. Noise attenuation for PTF $f = 1.0$ kHz, $\varsigma = 0.5$, a. $\gamma = 10^0$, b. $\gamma = 20^0$. [G.R.24]

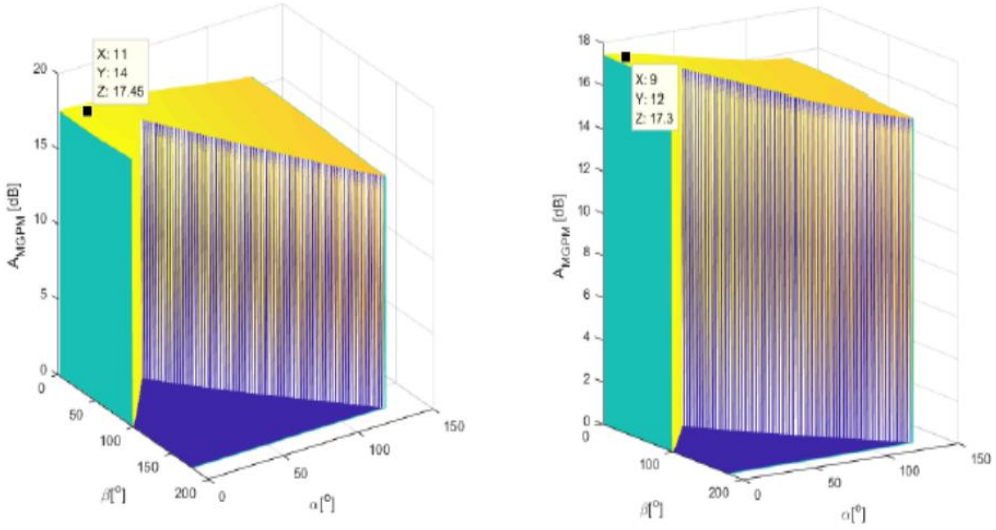

a) b)

Fig. 5.17. Noise attenuation for PTF f=1.0kHz, ς=0.5, a γ = 35^0, b. γ = 50^0[G.R.24]

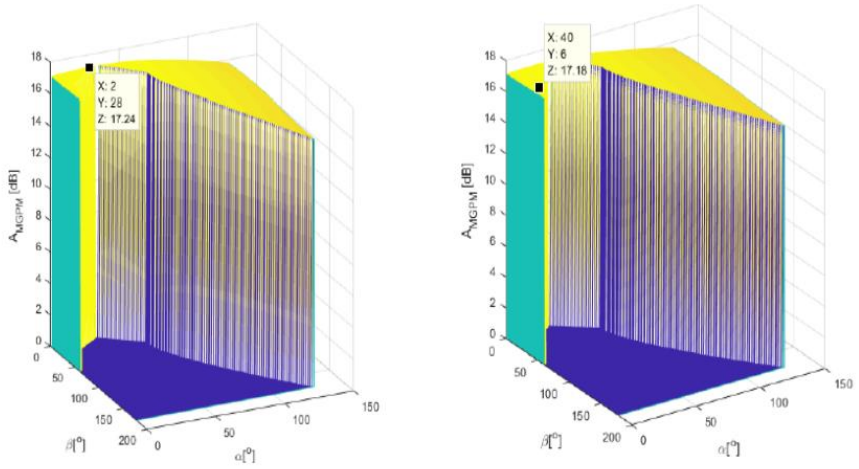

Fig. 5.18. Noise attenuation for PTF f=1.0kHz, ς=0.9, a γ = 10^0, b. γ = 20^0[G.R.24]

As can be seen from Figures 5.16-5.19, for the first case of the investigation, respectively for $x_R = 25.0\,\text{m}$, the sound's PTF $f = 1.0\,\text{kHz}$, the EFRG $\sigma_e = 1.0 \cdot 10^5$ Pa·s·m^{-2}, $\varsigma = 0.5, 0.9$ and the angles range $\alpha \in \left[1^0, 129^0\right], \gamma \in \left[1^0, 51^0\right], \beta \in \left[1^0, \beta_{max}\right]$ (for β_{max} see (5.16)), the maximum attenuation has the value of 17.64 dBA and is obtained for $\varsigma = 0.5$, $\alpha = 25^0, \beta = 9^0, \gamma = 10^0$, (see Fig. 516. a.). Analyzing Figures 5.16-5.19, it is evident that the ratio $\varsigma = h/a$ has a minor influence on the noise attenuation using an SIATRB with an AED mounted on the top.

Figures 5.20-5.24 illustrate the noise attenuation for the second case considering $x_R = 25.0\,\text{m}$, the sound's PTF $f = 1.0\,\text{kHz}$, the EFRG $\sigma_e = 1.0 \cdot 10^5$ Pa·s·m^{-2}, $\varsigma = 0.5$ and the angles range $\alpha \in \left[130^0, 175^0\right], \gamma \in \left[50^0, 5^0\right], \beta \in \left[1^0, 179^0\right]$, the ratio adopted to minimize the costs [G.R.24].

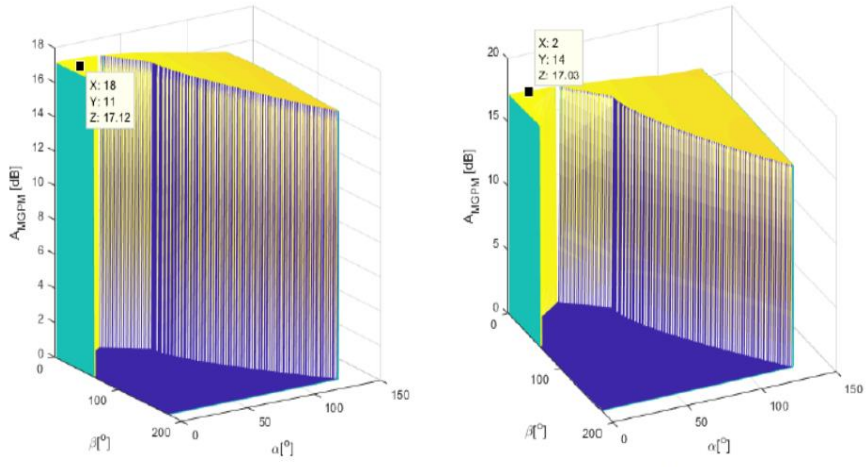

a) b)

Fig. 5.19. Noise attenuation for PTF f=1.0kHz, ς=0.9, a γ = 35^0, b. γ = 50^0[G.R.24]

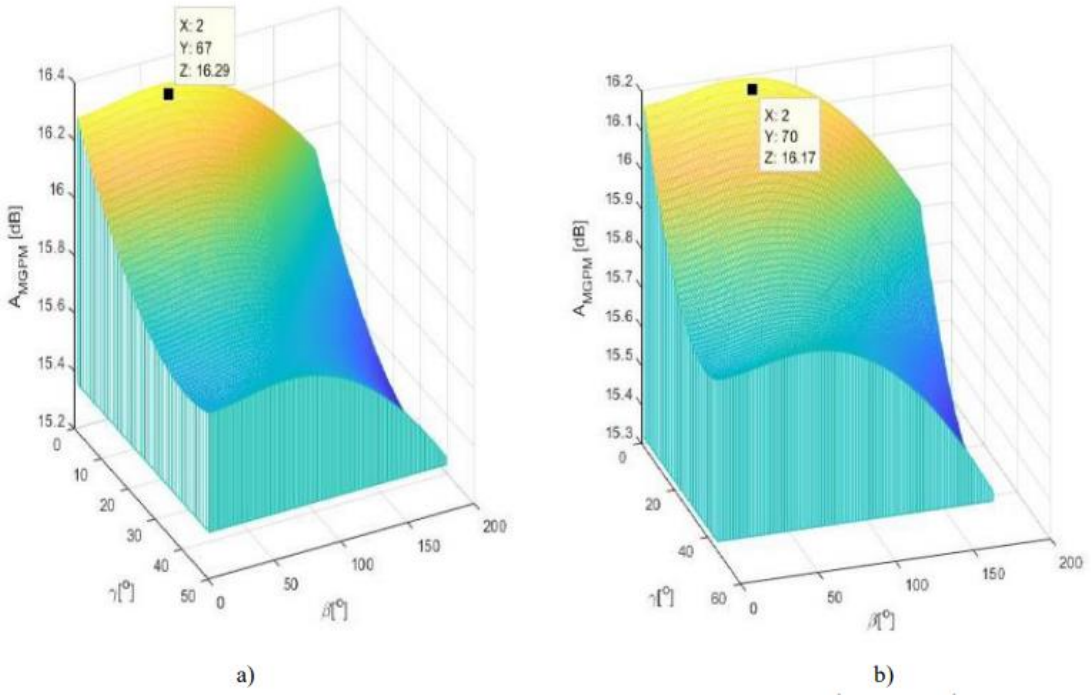

Fig. 5.20. Noise attenuation for PTF f=1.0kHz, ς=0.5, a $\gamma = 130^0$, b. $\gamma = 135^0$[G.R. 24]

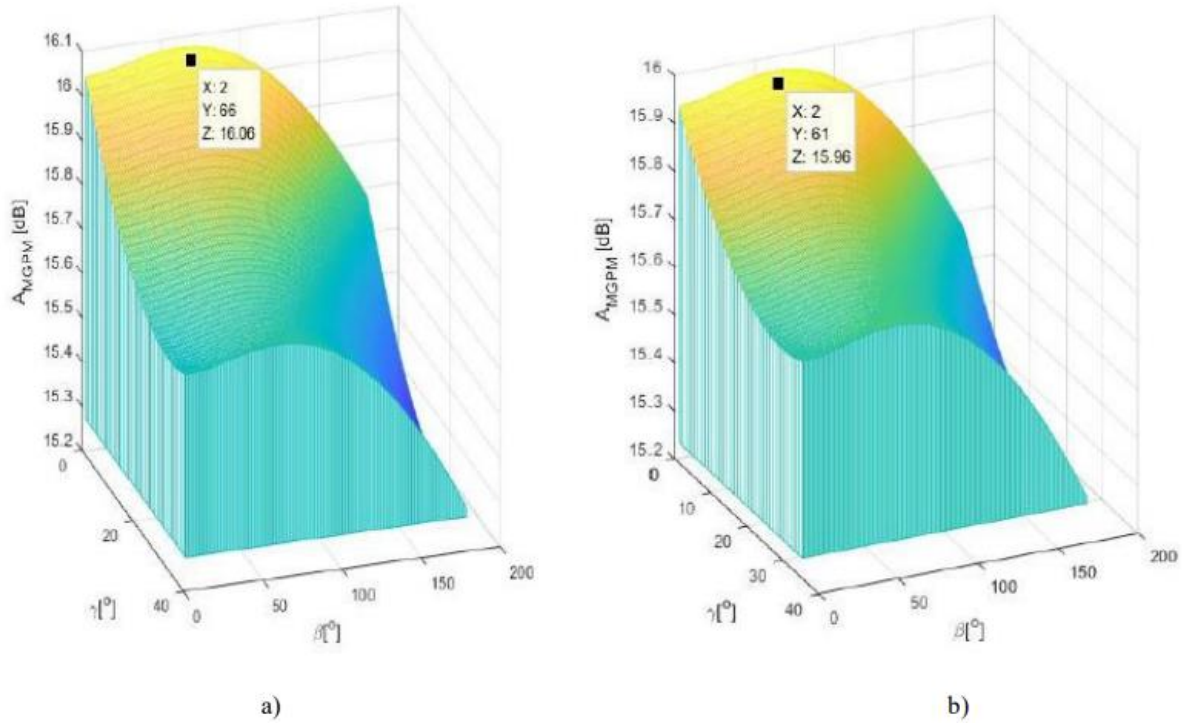

Fig. 5.21. Noise attenuation for PTF f=1.0kHz, ς=0.5, a $\gamma = 140^0$, b. $\gamma = 145^0$[G.R. 24]

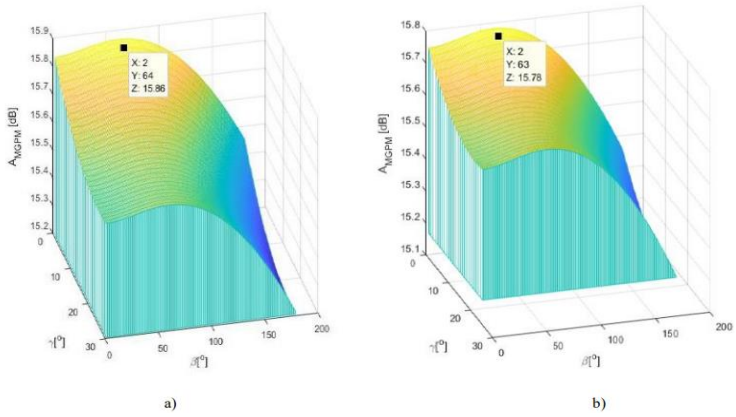

Fig. 5.22. Noise attenuation for PTF f=1.0kHz, ς=0.5, a γ = 150^0, b. γ = 155^0[G.R. 24]

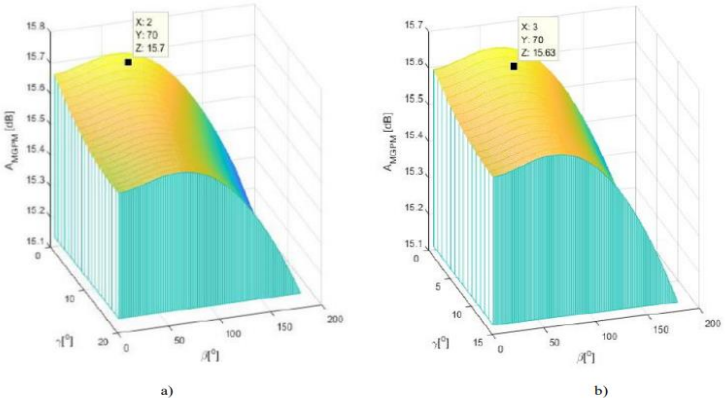

Fig. 5.23. Noise attenuation for PTF f=1.0kHz, ς=0.5, a γ = 160^0, b. γ = 165^0[G.R. 24]

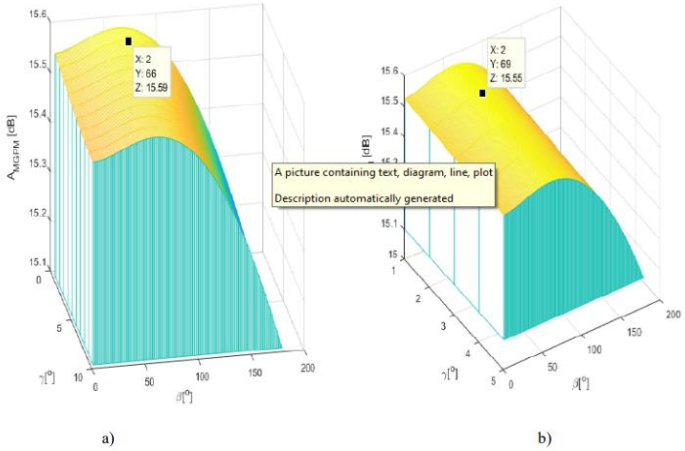

Fig. 5.24. Noise attenuation for PTF f=1.0kHz, ς=0.5, a γ = 170^0, b. γ = 175^0[G.R. 24]

Analyzing Figures 5.20 - 5.24, it is evident that the maximum noise attenuation has the value of 16.29 dBA, which is obtained for the values $\varsigma = 0.5$, $\alpha = 130^0, \beta = 67^0$, $\gamma = 2^0$ (see Figure 7. a.). This noise attenuation value is inferior with more than 1.3 dBA than the maximum value for the first case, which is 17.64 dBA (see Figure 5.20. a.). Considering the values of the angles, the variation of the noise attenuation, and the practical possibility of realizing such an AED, the optimal geometry to obtain the maximum noise attenuation of at least 17.6 dBA at 25 m distance from the SIATRB for a monopole noise having the PTF f =1.0 kHz is a=0.2 m, h=0.1 m, $\alpha = 25^0, \beta = 9^0, \gamma = 10^0$. The results agree with the data published in the literature[R.C.5.1; R.C.5.3]. Figure 5.25 illustrates the AARTNA of an SIATRB (having H=4.0 m) with an AED mounted on the top, with geometry characteristics a=0.2 m, h=0.1 m, $\alpha = 25^0, \beta = 9^0, \gamma = 10^0$, for the PTF in the range $f \in [0.1,3.0]$ kHz and the receiver having the coordinates $x_R \in [0.5,100.0]$ m, $y_R = 1.5$ m.

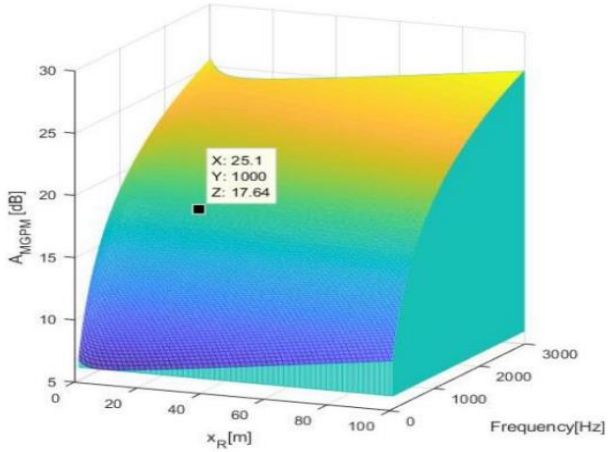

Fig. 5.25 Noise attenuation for SIATRB with an AED mounted on the top [G.R. 24]
$\alpha = 25^0, \beta = 9^0, \gamma = 10^0$, H=4m, a=0.2m, h=0.1m, x_R =3m, $y_S = 0.4m$, $x_R \in [0.5,100]m$, $y_R = 1.5m$

If we compare the results presented in Figure 5.25 with those in the literature[R.C.5.1; R.C.5.3], it can be remarked the agreement. The investigations carried out on the AED mounted on the top of an SIATRB reveal that the noise attenuation is obtained not only at high frequencies but also at low frequencies showing that this kind of edge diffraction is convenient for AARTNA. Also, the method used for the investigations, respectively the modified version of MGPM, indicates the need to improve ISO standards in the field, more precisely, ISO 96312-2 The investigations carried out on the AED mounted on the top of an SIATRB reveal that the noise attenuation is obtained not only at high frequencies but also at low frequencies showing that this kind of edge diffraction is convenient for AARTNA. Also, the method used for the investigations, respectively the modified version of MGPM, indicates the need to improve ISO standards in the field, more precisely, ISO 96312-2[G.R.17]. Another original contribution brought by the paper is using the new concept of *multiple acoustic diffractions* [R.C.5.2] in the optimization theory for AED. Considering a noise attenuation objective of 17.6 dBA at a 25 m distance from the SIATRB for a monopole noise having the PTF f =1.0 kHz for $\varsigma = 0.5$,it yields the angles $\alpha = 25^0, \beta = 9^0, \gamma = 10^0$, using the method designed previously. The results agree with the data published in the literature[R.C.5.1; R.C.5.3].

Chapter 6. Final conclusions. Directions for future research

6.1. Final conclusions

As can be seen by reading this Ph. D. thesis, the goals mentioned in Chapter One were achieved, respectively:

1. the design and development of an improved method to predict the noise attenuation, noise generated by automotive/railway traffic using semi-infinite thin rigid acoustic barriers, respectively MGPM (see chapters 4 and 5) method that includes the supplementary effects: the meteorological effects that imply the modifications of the Fresnel's numbers N_1, N_2, the effect of atmospheric absorption based Larsson's model [G.R. 14] (ISO 9613-1[R.C. 4.9]), effects of ground reflections-absorptions based on Delaney-Bazley model[G.R. 13] and the effect of attenuation generated by geometric divergence [G.R. 8, G.R. 12], compared to the classic GPM described by ISO 9613-2[R.C. 4.9];
2. optimization of symmetric edge diffraction, mounted on the top of the semi-infinite thin rigid acoustic barrier, using the new MGPM, to increase the attenuation of the noise generated by automotive/railway traffic [G.R. 8];
3. optimization of asymmetric edge diffraction, mounted on the top of the semi-infinite thin rigid acoustic barrier, using the new MGPM, to increase the attenuation of the noise generated in industrial areas [G.R. 19];
4. optimization of asymmetric edge diffraction, mounted on the top of the semi-infinite thin rigid acoustic barrier, using the new MGPM, to increase the attenuation of the noise generated by automotive/railway traffic [G.R. 23, G.R. 24].

The simulation data obtained using the new MGPM to realize the optimization of symmetric edge diffraction are in agreement with the experimental data published in the literature [G.R. 16, G.R. 18], and for the optimization of asymmetric edge diffraction mounted on the top of the semi-infinite thin rigid acoustic barrier, using the new MGPM, to increase the attenuation of the noise generated by automotive/railway traffic the results are also in agreement with the experimental data published in the literature [R.C.5.1, R.C.5.2].

The experimental data presented in Chapters 2 and 3 contribute to the comprehension and the modeling of the phenomena of multiple diffraction presented in Chapters 4 and 5 used to the optimization process of the symmetric and asymmetric edge diffraction mentioned previously at points 2-4.

6.2. Contributions

The most important contributions of this Ph.D. thesis are:

1. the design and development of an improved method to predict the noise attenuation, noise generated in industrial areas as well as by automotive/railway traffic using semi-infinite thin rigid acoustic barriers, respectively ***MGPM***;
2. the introduction of the next effects to predict the noise attenuation: the meteorological effects that imply the modifications of Fresnel's numbers N_1, N_2, the effect of atmospheric absorption based Larsson's model [G.R. 14] (ISO 9613-1[R.C. 4.9]), effects of ground reflections-absorptions based on Delaney-Bazley model[G.R. 13] and the effect of attenuation generated by geometric divergence [G.R. 8, G.R. 12];

3. optimization of symmetric edge diffraction, mounted on the top of the semi-infinite thin rigid acoustic barrier, using the new MGPM, to increase the attenuation of the noise generated by automotive/railway traffic [G.R. 8];
4. optimization of asymmetric edge diffraction, mounted on the top of the semi-infinite thin rigid acoustic barrier, using the new MGPM, to increase the attenuation of the noise generated in industrial areas [G.R. 19];
5. optimization of asymmetric edge diffraction, mounted on the top of the semi-infinite thin rigid acoustic barrier, using the new MGPM, to increase the attenuation of the noise generated by automotive/railway traffic [G.R. 23, G.R. 24].

6.3. Directions for future research

The new method MGPM was tested only for pure tones in the frequency range [100 . . . 4000] Hz, one of the future research directions is the test in 1/3 of the octave in the frequency range [0.100 . . . 16.000] kHz.

Another research direction is the use of multi-pole sources for automotive noise traffic and for railway noise traffic. In this way, the noise generated by the impact between the wheel and the road (using a quadrupole for vehicles and a multiple-line source for the railway) will be better simulated using 3D models.

As can be remarked from the previous aspect the simulations must include the 3D geometry for the multi-pole source disposal when enhancing the new MGPM. Also, it must be considered that the noise sources are in movement with respect to the acoustic barrier that is fixed, the speed being stationary or transitory. The last two aspects are also new future research directions.

References

General References

1.- Bugaru, M., Enescu, N., Stanila, R., Vasile, O., Reflection and absorption of the acoustical barriers of finite length, Proceedings of 12th International Congress on Sound and Vibration, ICSV 2005, Lisbon, Portugal, 2005, Vol. 3, pp. 2143-2149, ISBN 978-162748149-6, Scopus Indexed, https://www-scopus-com.am.e-nformation.ro/record/display.uri?eid=2-s2.0-84881575176&origin=resultslist&sort=plff&src=s&st1=BUGARU&st2=Mihai&nlo=1&nlr=20&nls=countf&sid=ad5f4e3c8b353a67f99317754b89466c&sot=anl&sdt=aut&sl=31&s=AUID%28%22Bugaru%2c+M.%22+13805674800%29&relpos=16&citeCnt=0&searchTerm=&featureToggles=FEATURE_NEW_DOC_DETAILS_EXPORT:1

2.- Vasile O., "Insertion Loss Analysis of the Acoustic Panels with Composite Construction", pp. 85-91,Analele Universității "Eftimie Murgu", Anul XX, nr. 2, 2013, ISSN 1453-7397. (CNCSIS B+/ BDI:EBSCO, DOAJ, RePEc, ProQuest, ICAAP, Ulrich's, IndexCopernicus, Livre, Academic Journals Database, NewJour

3.- Rossing Th.D.Springer Handbook of Acoustics – Stanford University- Center for Computer Reserch in Music and Aacoustic-Stanford CA94305 USA- ISBN:978-0-387-30446-5; e-ISBN:0-387-30425-0
https://link.springer.com/referencework/10.1007/978-0-387-30425-0

4. - SR EN 1794-1 – Road traffic noise reducing devices – Non-acoustics performance. Part 1: Mechanical performance and stability requirements.
https://standards.iteh.ai/catalog/standards/cen/b9f56d54-37ce-48a4-ae93-725e689b5e36/en-1794-1-2018

5. - CR 1-1-4:2012 - Design code. Evaluation of the wind action on constructions.
https://www.scribd.com/document/259194806/Romanian-Wind-Code-CR1-1-4#

6.- Bugaru, M., Dale, R., Acoustic properties of sound barriers, Proceedings of the 14th International Congress on Sound and Vibration, ICSV 2007, Cairns, Australia, 2007, Vol. 5, pp. 4244-4250, ISBN 978-162748000-0, Scopus Indexed, https://www-scopus-com.am.e-nformation.ro/record/display.uri?eid=2-s2.0-84881402979&origin=resultslist&sort=plff&src=s&st1=BUGARU&st2=Mihai&nlo=1&nlr=20&nls=countf&sid=ad5f4e3c8b353a67f99317754b89466c&sot=anl&sdt=aut&sl=31&s=AU-ID("Bugaru%2c+M."+13805674800)&relpos=5&citeCnt=0&searchTerm=&featureToggles=FEATURE_NEW_DOC_DETAILS_EXPORT:1

7.- Bugaru M., Zaharia, M. C., Chereches, T., Arsene, M., (2008), Multi-layered phono-insulated and phonoabsorbing acoustic barrier- Invention Patent, Official Bulletin of Industrial Property, OSIM, RO-BOPI No.03/2010 Romanian PATENT no. 122864/2010.

8.- Bugaru, M., Vasile, O., **Neagoe, M.,** Recent Developments of Noise Attenuation Using Acoustic Barriers for a Specific Edge Geometry, MDPI-Computation, e-ISSN 2079-3197, **2021**, Vol 9, 9(12)-129, **WOS: 000736262800001**, DOI: 10.3390/computation9120129, https://doi.org/10.3390/computation9120129,

https://www.webofscience.com/wos/woscc/fullrecord/WOS:000736262800001?SID=EUW1ED0BAEcWoqNMuNgqJY88vtNwz
9. - Maekawa, Z.(1968) „Noise reduction by screens." Appl. Acoustics . Vol.1,no.3, pp. 157–173. https://www.sciencedirect.com/science/article/abs/pii/0003682X68900200?via%3Dihub
10. -Tatge, R.B.(1973) „Barrier-wall attenuation with a finite sized source." Journal of the Acoustical. Society of America vol.53, no.5 pp. 1317–1319.11. -Kurze, U.J.; Anderson, G.S.(1971)," Sound attenuation by barriers" Applied Acoustics vol.4, no.1,pp. 35–53, https://www.sciencedirect.com/science/article/abs/pii/0003682X71900247
12. -Menounou, P. (2001) „A correction to Maekawa's curve for the insertion loss behind barriers." The Journal of the Acoustical. Society of America, Vol.110, no.3 pp.1828–1838, https://pubs.aip.org/asa/jasa/article-abstract/110/4/1828/547382/A-correction-to-Maekawa-s-curve-for-the-insertion?redirectedFrom=fulltext
13. -Delany, M.E.; Bazley, E.N.(1970)" Acoustical properties of fibrous absorbent materials". Applied. Acoustics Vol.3, no.2 pp. 105–116.
https://www.sciencedirect.com/science/article/abs/pii/0003682X70900319?via%3Dihub
14. -Larsson, C.(1997)," Atmospheric Absorption Conditions for Horizontal Sound Propagation." Applied. Acoustics, Vol.50, no.3, pp. 231–245.
https://www.sciencedirect.com/science/article/abs/pii/S0003682X96000680?via%3Dihub
15. International Standard Organization. ISO 9613-1(1993): Acoustics: Noise Absorption by Air. Attenuation of Sound during Propagation Outdoors. Part 2: Calculation of the Absorption of Sound by the Atmosphere; International Standard Organization: Geneva,Switzerland,
https://www.iso.org/obp/ui/en/#iso:std:iso:9613:-1:ed-1:v1:en
16.- Karimi, M., Younesian, D., (2014), "Optimized T-Shape and Y-Shape Inclined Sound Barriers for Railway Noise Mitigation", Journal. of Low-Frequency Noise, Vibration and Active Control, Vol.33,no.3 pp. 357-370.
https://journals.sagepub.com/doi/10.1260/0263-0923.33.3.357
17. International Standard Organization. ISO 9613-2(1996): Acoustics: Attenuation of Sound During Propagation Outdoors. Part 2: General Method of Calculation (International Standard Organization, Geneva, Switzerland).
https://www.iso.org/standard/20649.html
18. - Ishizuka, T. , Fujiware, K.(2004)" Performance of noise barriers with various edge shapes and acoustical conditions", Applied Acoustics, Vol. 65, no.2 pp.125-141
Performance of noise barriers with various edge shapes and acoustical conditions - ScienceDirect
19 - Bugaru, M., Vasile, O., **Neagoe, M**., Optimization of a Specific Edge Diffraction for Industrial Areas Using the MGPM, Proceedings of the 10th IC-SCCE, 10th International Conference from Scientific Computing to Computational Engineering, 6-9 July 2022, Athens, Greece, ISSN 2241-8865, ISBN 978-618-84028-4-3, pp. 170-178
20. - Bugaru, M., Vasile,O., **Neagoe, M**., ANALYSIS OF NOISE REDUCTION AND THE INFLUENCE OF WAVE'S DIFFRACTION ANGLE USING NOISE BARRIERS, Acta Technica Napocensis, Series: Applied Mathematics, Mechanics and Engineering, ISSN 1221-

5872, 2022, Vol. 65, Issue, 1, pp. 29-36, **WOS:000832312500005**,
https://www.webofscience.com/wos/woscc/full-record/WOS:000832312500005
21.- Neagoe, M .,Bugaru, M., Vasile, O.(**2021**), "Analysis of noise reduction and the influence of wave's diffraction angle using noise barriers", 9th International Conference from "Experiments/Process/System Modeling/Simulation/Optimization" 9th IC-EPSMSO Athens, 7-10 July, 2021 ©LFME pp.57-65
22.- Bugaru, M., **Neagoe, M**., Vasile, O., Recent developments of noise attenuation using acoustic barriers for a specific edge geometry, 9th International Conference on "Experiments/Process/System Modeling/Simulation/Optimization",9th IC-EPSMSO, Athens, Greece, 7-10 July **2021**, pp. 271-279, ISSN: 2241-9209, ISBN: 978-618-84028-2-9
23.- Bugaru, M., **Neagoe M**. (**2023**) " Analysis of antisymmetric edge diffraction for acoustic barriers designed for automotive and railway traffic noise attenuation" 10th International Conference on "Experiments/Process/System Modeling/Simulation/Optimization" Athens,5-8 July 2023 pp.20-29
24. - Bugaru, M., **Neagoe M**. (2023) " Investigation of asymmetric edge diffraction for acoustic barriers" U.P.B. Sci. Bull., Series D, Vol. …, Iss. …, 2023 ISSN 1454-2358 (în curs de publicare)

References Chapter 1

1. – CEEX, Modulul I, A6761/2006, 2006-2008, nr. int. 31-06-05, Cercetări avansate privind reducerea nivelului poluării sonore, în zonele locuite, generată de traficul feroviar și rutier, prin amplasarea de bariere acustice, CO: UPB,P1:ATM,P2:INCERC,P3:S.C.Afico S.A.- Director responsabil contract :prof. unv. dr. ing. Bugaru M.
2. - https://eur-lex.europa.eu/legal content/RO/TXT/PDF/?uri=CELEX:52017DC0151&from=EN
3.- http://ier.gov.ro/wp-content/uploads/publicatii/Pais1_studiu_B1-2_ro.pdf
4. - Moser M.- Engineering Acoustics- An Introduction to Noise Control - Second Edition – ISBN 978-3-540-92722-8; e-isbn 978-3-540-92723-5 Springer Dordrecht Heidelberg London New York Engineering Acoustics: An Introduction to Noise Control | SpringerLink
5. - Sandberg U., Will tire / road noise limit future vehicle noise reductions?, Proceedings of Inter Noise 1982, San Francisco, USA, 1982.
6. - Enescu N., Vasile O., The Decrease of Noise with Acoustics Barriers, Romanian Journal of Acoustics and Vibration, Vol. IV, Number 2, December 2007, pp. 71-74, ISSN 1584-7284 https://www.academia.edu/1128592/The_Decrease_of_Noise_with_Acoustics_Barriers
7. – Pascu C, Badea G., Lepadatu I.; C.D.Comeaga, Sound-absorbing and sound-insulating modular panel for noise barriers, Proceedings of CEEX Conference ISBN 978-973-0-05258-9 Edited by A.Voicilă, D. Cuniță, A.Eșanu, E.Fileru – UCP AMTRAS – Bucharest, Nov. 2007, p75-78(inRomanian)
8.- https://mfinante.gov.ro/documents/35673/980619/sausticsi678541_12022021.pdf
9. - LEIER ROM S.R.L. ; Dispozitive pentru reducerea zgomotului produs de traficul rutier și feroviar - panouri fonoizolante din elemente durisol - Infrastructura de transport protecție împotriva zgomotului 23 – 24.09.2014, București
https://www.leier.ro/panouri-fonoizolante-durisol/

10. - Universitatea.Politehnică.București.- Teză de doctorat – Materiale compozite ecologice destinate reducerii zgomotului – 2012 – drd. Ing. Bratu Mihai
http://dspace.incdecoind.ro/bitstream/123456789/456/1/Rezumat_teza_Mihai%20BRATU.pdf
11.- https://xdocs.ro/doc/reabilitarea-acustica-cursul-7ppt-6nw56rxrx2n1

References Chapter 2

1 - EN 14388:2016 – Specifications. Road traffic noise reducing devices.
https://www.en-standard.eu/une-en-14388-2016-road-traffic-noise-reducing-devices-specifications/
2.- Bratu, M., Bucur, E., Danciulescu, V., Petrescu, M., Gheorghita, T., Vasile, O. (2020), Assessment of the level of noise and chemical air pollution in two distinct urban areas, http://Doi.Org/10.21698/ Rjeec.2020.216
https://www.researchgate.net/publication/346277127_Assessment_of_the_level_of_noise_and_chemical_air_pollution_in_two_distinct_urban_areas
3.- Karakitsios, S.P., Papaloukas, C.L., Kassomenos, P.A., Pilidis, G., Assessment and prediction of benzene concentrations in a street canyon using artificial neural networks and deterministic models: their response to "what if" scenarios,
http://Doi.Org/ 10.1016/J.Ecolmodel.2005.07.024.
https://www.sciencedirect.com/science/article/abs/pii/S0304380005003984
4.- Sygna, K., Aasvang, G.M., Aamodt, G., Oftedal, B., Krog, N.H., Road traffic noise, sleep and mental health, http://Doi.Org/ 10.1016/J.Envres.2014.02.010.
https://pubmed.ncbi.nlm.nih.gov/24637180/
5.- Begou, P., Kassomenos, P., Kelessis, A., Effects of road traffic noise on the prevalence of cardiovascular diseases: the case of Thessaloniki, Greece,
http://Doi.Org/ 10.1016/J.Scitotenv.2019.134477.
https://www.sciencedirect.com/science/article/abs/pii/S0048969719344687
6.-https://envi.ro/wp-content/uploads/2019/08/Utilizarea_noului_analizor_tip_2270.pdf
7. - Piechowicz, J. (2011), "Sound Wave Diffraction at the Edge of a Sound Barrier", Acta Physica Polonica Series A 119(6A), DOI:10.12693/APhysPolA.119.1040
https://www.researchgate.net/publication/266881035_Sound_Wave_Diffraction_at_the_Edge_of_a_Sound_Barrier
8. - CR 1-1-3:2012 - Design code. Evaluation of the action of snow on constructions.
https://www.matrixrom.ro/en/produs/cr-1-1-3-2012-design-code-evaluation-of-the-action-of-snow-on-constructions-supplement-calculation-examples-design-recommendations/
9.- Tămaş-Gavrea, D.-R.; Dénes, T.-O.;Iştoan, R.; Tiuc, A.E.; Manea, D.L. Vasile,
O., A novel acoustic sandwich panel based on sheep wool, Coatings, http://Doi.Org/10.3390/ Coatings10020148.
https://www.mdpi.com/2079-6412/10/2/148
10.- Jin, Y., Fang, X., Li, Y, Torrent, D.,Engineered diffraction gratings for acoustic cloaking, http://Doi.Org/10.1103/Physrevapplied.11.011004.
https://journals.aps.org/prapplied/abstract/10.1103/PhysRevApplied.11.011004

11.- Pirinchieva, R.K., The influence of barriersize on its sound diffraction, http://Doi.Org/ 10.1016/0022-60x(91)90570-A
https://www.sciencedirect.com/science/article/abs/pii/0022460X9190570A

References Chapter 3

1 - SR EN 14388:2008 , Dispozitive de reducere a zgomotului din traficul rutier. Specificații
https://www.scribd.com/document/140021924/SR-EN-14388-AC-2008-Dispozitive-de-Reducere-a-Zgomotului-Din-Traficul-Rutier-Specificatii
2 - SR EN 1793-1: 2017 Dispozitive pentru reducerea zgomotului din traficul rutier. Metoda de încercare pentru determinarea performanței acustice.
https://magazin.asro.ro/ro/standard/254365
3 - SR EN 14389-1:2015 Dispozitive de reducere a zgomotului.Proceduri de evaluare a performanțelor pe termen lung
https://standards.iteh.ai/catalog/standards/cen/e2bbd859-2b47-491e-8ffc-c6a24567f660/en-14389-1-2015
4- SR EN 1793-2: 2018 Dispozitive pentru reducerea zgomotului din traficul rutier. Metoda de încercare pentru determinarea performanței acustice.
https://www.en-standard.eu/bs-en-1793-2-2018-road-traffic-noise-reducing-devices-test-method-for-determining-the-acoustic-performance-intrinsic-characteristics-of-airborne-sound-insulation-under-diffuse-sound-field-conditions/

References Chapter 4

1 -Smith, M. Barriers to consistent results: The effects of weather. In Proceedings of the ACOUSTICS, AAS'08, Geelong, VIC, Australia, 24–26 November 2008; Acoustics and Sustainability; pp. 1–5.
https://www.semanticscholar.org/paper/Barriers-to-consistent-results%3A-the-effects-of-Smith/d57ad1570b97e07b1321b105bcfbfd8cd9c2058f
2 -International Standard Organization. ISO 9613-2: Acoustics: Attenuation of Sound during Propagation Outdoors. Part 2: General Method of Calculation; International Standard Organization: Geneva, Switzerland, 1996.
https://www.iso.org/standard/20649.html
3 -H.E. Bass, L.C. Sutherland, A.J. Zuckewar: Atmospheric absorption of sound: Further developments, J. Acoust. Soc. Am. 97, 680–683 (1995)
https://pubs.aip.org/asa/jasa/article-abstract/97/1/680/835919/Atmospheric-absorption-of-sound-Further?redirectedFrom=fulltext
4 -Heinrich Kuttruf:Acoustics –An introduction-this edition published in the Taylor and Francis 2006 ISBN 0-203-97089-6
https://www.taylorfrancis.com/books/mono/10.1201/9780367807696/acoustics-heinrich-kuttruff
https://www.academia.edu/7130258/Acoustics_An_introduction_Heinrich_Kuttruff_Taylor_and_Francis_English_Edition_2007_Paperback_XIII_478_pages_ISBN_978_0_415_38680_7

5 -SR ISO 10847 - Acoustics – In-situ determination of insertion loss of outdoors noise barriers of all types.58
https://www.iso.org/standard/1314.html
6 –Bugaru M.*, Enescu N.*, Vasile O.*, Raluca Nicoleta Stanila* Specific noise attenuation with acoustic barriers - International Conference on Experiments/Process/System Modelling/Simulation/Optimization 1st IC-EpsMsO Athens, 6-9 July, 2005
https://www.researchgate.net/publication/258211988_Reflection_and_absorption_properties_of_the_acoustical_barriers_of_finite_length
7 -Michael Moser - Engineering Acoustics- An Introduction to Noise Control - Second Edition – ISBN 978-3-540-92722-8; e-isbn 978-3-540-92723-5 Springer Dordrecht Heidelberg London New York
https://link.springer.com/book/10.1007/978-3-540-92723-5
8 - F. Alton Everest- The Master Handbook of Acoustics –fourth edition
https://www.accessengineeringlibrary.com/content/book/9780071360975
9 - ISO 9613-1: Acoustics: Noise Absorption by Air. Attenuation of sound during propagation outdoors. Part 2: Calculation of the absorption of sound by the atmosphere (International Standard Organization, Geneva, Switzerland 1993).
https://www.iso.org/standard/17426.html
10- Bugaru, M., Zaharia, M. C., Chereches, T., Arsene, M., (2008), Multi-layered phono-insulated and phonoabsorbing acoustic barrier, Romanian PATENT no. 122864/2010.

References Chapter 5

1. Okubo, T., Fujiwara, K.(1999), "Efficient of a noise barrier with an acoustically soft cylindrical edge for practical use", in The Journal of the Acoustical Society of America,Vol. 105, no. 6, pp. 3326-3335.
https://pubs.aip.org/asa/jasa/article-abstract/105/6/3326/553411/Efficiency-of-a-noise-barrier-with-an-acoustically?redirectedFrom=fulltext
2. Pardo-Quiles, D., Rodriguez, J.V.(2020), "A Fast UTD-Based Method for the Analysis of Multiple Acoustic Diffraction over a Series of Obstacles with Arbitrary Modeling, Height and Spacing", Symmetry-MDPI, Vol. 12, no. 654, pp. 1-24.
https://www.mdpi.com/2073-8994/12/4/654